Published for SISSA by Springer

Received: *August 8, 2023*
Accepted: *November 10, 2023*
Published: *November 22, 2023*

BSM patterns in scalar-sector coupling modifiers

Christoph Englert, Wrishik Naskar and Dave Sutherland

School of Physics & Astronomy, University of Glasgow, University Avenue, Glasgow G12 8QQ, United Kingdom

E-mail: christoph.englert@glasgow.ac.uk, w.naskar.1@research.gla.ac.uk, david.w.sutherland@glasgow.ac.uk

Abstract: We consider what multiple Higgs interactions may yet reveal about the scalar sector. We estimate the sensitivity of a Feynman topology-templated analysis of weak boson fusion Higgs pair production at present and future colliders — where the signal is a function of the Higgs coupling modifiers κ_V, κ_{2V}, and κ_λ. While measurements are statistically limited at the LHC, they are under general perturbative control at present and future colliders, departures from the SM expectation give rise to a significant future potential for BSM discrimination in κ_{2V}. We explore the landscape of BSM models in the space of deviations in κ_V, κ_{2V}, and κ_λ, highlighting models that have measurable order-of-magnitude enhancements in either κ_{2V} or κ_λ, relative to their deviation in the single Higgs coupling κ_V.

Keywords: Compositeness, Higgs Production, Higgs Properties, Multi-Higgs Models

ArXiv ePrint: 2307.14809

https://doi.org/10.1007/JHEP11(2023)158

JHEP11(2023)158

Contents

JHEP11(2023)158

1 Introduction

The so-called κ framework that has been put forward in parallel to the Higgs boson discovery [1] to assist its characterisation programme has proved a helpful tool in gaining a qualitative understanding of Higgs boson physics. The modifier for a coupling g present in the Standard Model (SM) $g = g_{\rm SM}$ is defined as

$$\kappa_g = \frac{g}{g_{\rm SM}}\,. \tag{1.1}$$

The κ framework traces modifications of the Lorentz structures present in the SM exclusively. This leads to violation of gauge invariance with detrimental implications, which signifies the need to consider a more flexible theoretical setting. A comprehensive approach based on effective field theory (in its linear or non-linear realisations) elevates this programme to a better-grounded framework. Theoretical consistency plays an important role when more data becomes available at the Large Hadron Collider (LHC), thus enabling and necessitating a more detailed study of Higgs properties beyond tree level. Yet, practical considerations related to the LHC's sensitivity to certain coupling modifications leave the κ framework

still applicable in a range of processes. One such process is weak boson fusion (WBF) Higgs pair production, where the κ framework sees continued application. In, e.g., the recent [2], modifications of the (trilinear) Higgs self-coupling κ_λ and the quartic gauge-Higgs couplings κ_{2V} have been constrained

$$\kappa_\lambda \in [-3.5, 11.3]\,, \qquad \kappa_{2V} \in [0.0, 2.1]\,, \tag{1.2}$$

with similar sensitivity in other di-Higgs final state channels, e.g. [3–9]. The κ framework also successfully captures the dominant source of coupling modifications in many concrete UV extensions.

The Higgs self-coupling corresponds to a unique operator in the dimension 6 effective field theory expansion [10]. Modifications of $\kappa_\lambda \neq 1$ can therefore be housed theoretically consistently, which is also demonstrated by κ_λ investigations beyond tree level [11–14] that do not lead to theoretical inconsistencies.

This is vastly different for $\kappa_{2V} \neq 1$, which breaks electroweak gauge invariance in the SM(EFT), leading to a breakdown of renormalisability. As κ_{2V} is related to a modification of the gauge sector, a departure from $\kappa_{2V} = 1$ requires care when moving beyond tree-level considerations [15]. Notwithstanding these theoretical obstacles, the gauge-Higgs quartic interactions can be strong indicators of Higgs compositeness as a consequence of dynamical vacuum misalignment. For instance, in minimal theories of Higgs compositeness [16, 17], the typical deviations in the Higgs-gauge sector are given by

$$\kappa_V = \sqrt{1-\xi}\,, \quad \kappa_{2V} = 1 - 2\xi\,, \tag{1.3}$$

where ξ measures the electroweak vacuum expectation value $v \simeq 246$ GeV in units of the CCWZ [18, 19] order parameter. These relations are independent of the mechanism responsible for vacuum misalignment; they are independent of how partial compositeness is included in the fermion sector. In contrast, for scenarios of iso-singlet mixing [20–23], we obtain

$$\kappa_V = \cos\alpha\,, \quad \kappa_{2V} = \cos^2\alpha\,. \tag{1.4}$$

It is immediately clear that a sufficiently precise measurement of the quartic gauge-Higgs coupling, κ_{2V}, serves as a discriminator between these two dramatically different BSM scenarios. While it is always possible to interpret $\kappa_V < 1$ in either scenario through identifying $\cos\alpha = \sqrt{1-\xi}$,

$$\cos 2\alpha \neq \cos^2\alpha \tag{1.5}$$

away from the decoupling limit $\alpha \neq 0 \neq \xi$ in either BSM scenario.

In this note, we provide a detailed discussion about the relevance of κ_{2V} and its relation to κ_V, κ_λ for BSM physics, spanning from traditional renormalisable scenarios to effective theories. We will focus on the phenomenology in WBF di-Higgs production at the LHC and its extrapolation to other future collider environments, where these three couplings enter on an a priori equal footing. Including a viewpoint of geometry [24], we clarify the sensitivity to BSM scenarios that can be gained in a range of models (and their deformations) at the high-luminosity (HL-)LHC phase, as well as future colliders such as the FCC-hh or

JHEP11(2023)158

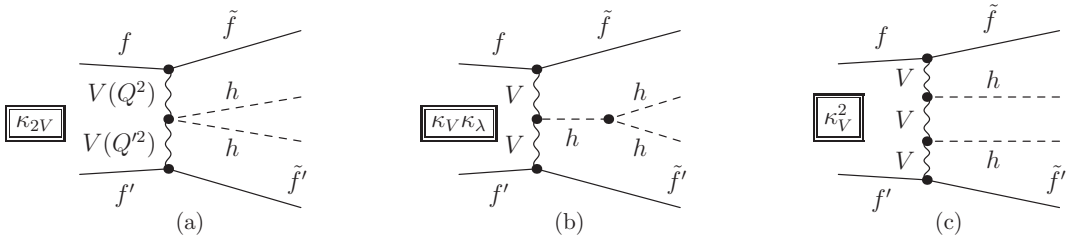

Figure 1. Representative Feynman diagram topologies contributing to κ_{2V} sensitivity via weak boson fusion.

electron-positron machines. In passing, we include a discussion of higher-order QCD effects at hadron machines.

This work is organised as follows: in section 2, we discuss the future sensitivity that can be achieved in a Feynman-diagram templated analysis as performed by the experiments, extrapolating from the current sensitivity that they report. This forms the phenomenological backdrop of the theoretical reach of this sensitivity in section 3. There we categorise the κ_V, κ_{2V}, κ_λ parameter space in terms of renormalisable theories and effective theories of compositeness and their deformations. We summarise in section 4, which provides an outlook towards monetising the BSM potential of κ_{2V} sensitivity in these experimental environments in relation to κ_V and κ_λ.

2 Present and future of scalar couplings in WBF Higgs pair production

In this section, we consider the experimental limit on κ_V, κ_{2V}, and κ_λ, as defined by the tree-level lagrangian

$$\mathcal{L} = \frac{1}{2}(\partial h)^2 + m_W^2 \left(W_\mu^+ W^{-\mu} + \frac{1}{2c_W^2} Z_\mu Z^\mu \right) \left[1 + \kappa_V \frac{2h}{v} + \kappa_{2V} \frac{h^2}{v^2} \right] - \kappa_\lambda \frac{m_h^2}{2v} h^3 \,, \quad (2.1)$$

with $v = 246$ GeV and cosine of the Weinberg angle $c_W = \cos\theta_W$. Tree-level custodial symmetry is assumed throughout (i.e., $\kappa_W = \kappa_Z = \kappa_V$ and $\kappa_{2W} = \kappa_{2Z} = \kappa_{2V}$).

Before we turn to the relevance of the different couplings and their BSM reach, it is instructive to clarify the anticipated shape of the $\kappa_V - \kappa_{2V}$ exclusion. WBF probes the incoming weak bosons at space-like momenta in the diagrams of figure 1. However, the analysis of $Wh \to Wh$ scattering for physical momenta (the crossed process that enters WBF subdiagrams of figure 1) provides insight into gauge-symmetry cancellations that carry over into qualitative phenomenological outcomes via the effective W approximation [25, 26]. In the high energy limit $\sqrt{s} \gg m_h + m_W$, the polarised amplitudes scale as[1]

$$\frac{m_W^2}{s} \mathcal{A}(W_L h \to W_L h) \sim \frac{m_W}{\sqrt{s}} \mathcal{A}(W_T h \to W_L h) \sim \kappa_{2V} - \kappa_V^2 \,. \quad (2.2)$$

[1]This result can be straightforwardly obtained with FeynArts/FormCalc/LoopTools [27–29], which we use throughout this work. Phase-space and polynomial suppression of the valence quark parton distribution functions significantly modify these naive expectations.

JHEP11(2023)158

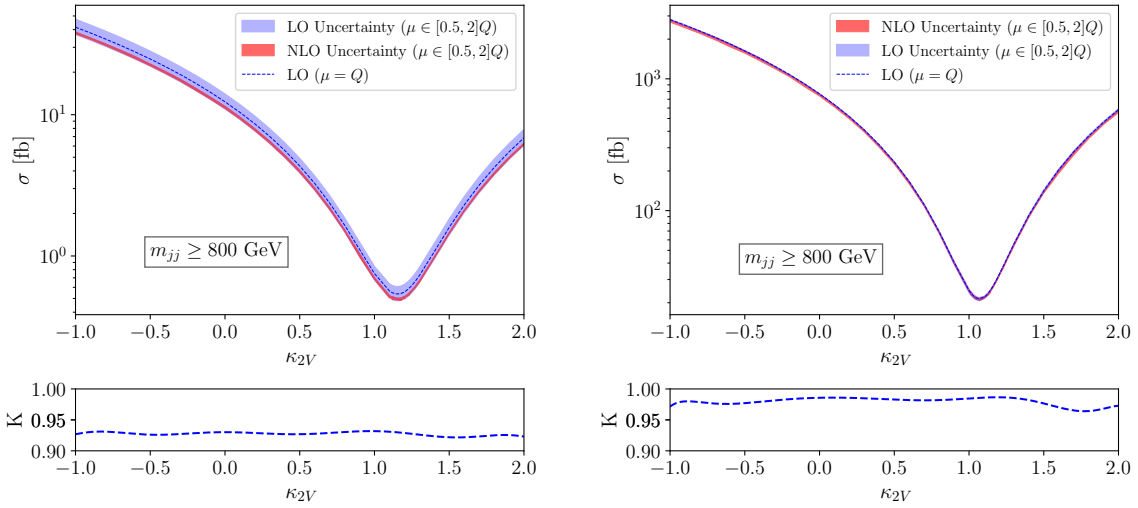

Figure 2. Next-to-leading order QCD corrections to WBF $pp \to hhjj$ production in the large invariant tagging jet mass region $m_{jj} \geq 800$ GeV at the LHC (a) and FCC-hh (b) as a function of κ_{2V} for all other parameters chosen to be SM-like.

This shows that in the SM (as well as for direct Higgs mixing), we can expect a significant destructive interference to maintain unitarity at high energies. The scaling with energy in the WBF process is pdf-suppressed for massless partons (including in the effective W approximation), however, large enough deviations from the SM correlation manifest themselves as an enhanced cross section so that limits can be set. Note that κ_λ does not enter the Wh amplitude with energy enhancement, and its constraints are therefore set by a priori perturbativity limits (see [30–32] for more model-specific considerations).

2.1 Hadron collider constraints on κ_V and κ_{2V}

$pp \to hhjj$ production follows hjj production from the point of view of QCD. Therefore, the search region that is selected by the LHC experiments exploits the usual WBF paradigm [33–36]. Similar to the findings in single-Higgs and double-Higgs production via WBF [37, 38], the QCD corrections can be formidably captured through an adapted choice of the renormalisation and factorisation scales, due to the process' 'double-Deep Inelastic Scattering' structure. In particular, in the κ_{2V} measurement region selected by the LHC experiments then becomes extraordinarily stable: in figure 2 we show the $pp \to hhjj$ WBF cross section component at next-to-leading order QCD in comparison to the leading order estimate, employing the central scale choice $\mu = Q$ (cf. figure 1) for the signal region characterised by an invariant jet mass of $m_{jj} \geq 800$ GeV.[2] This extends to the FCC-hh at a significantly increased cross-section, figure 2. The cross-section is well-approximated by the LO $\mu = Q$ choice, and the NLO corrections are modest $\sim 5\%$ at the LHC, decreasing in

[2]We obtain this through a modification of the publicly available VBFNLO Monte Carlo programme [36, 39, 40]. Modifications have been cross-checked against MADGRAPH_aMC@NLO [41]. See also [42] for studies of rescalings of the Higgs self-coupling.

JHEP11(2023)158

relevance at the FCC-hh, running at 100 TeV [43]. The key limitation of setting constraints on κ_{2V} is then statistics and background systematics.

The ATLAS Collaboration has previously published search results for nonresonant $hh \to b\bar{b}b\bar{b}$ production using 27 fb^{-1} of early Run 2 data [44], as well as a dedicated search for VBF hh production in 126 fb^{-1} of data collected between 2016 and 2018 [45]. The latest analysis [2] builds upon these earlier results by incorporating the 2016–2018 data for both production channels and taking advantage of improvements in jet reconstruction and b-tagging techniques. Notably, the analysis employs an entirely data-driven technique for background estimation, utilising an artificial neural network to perform kinematic reweighting of data to model the background in the region of interest, and it currently restricts κ_{2V} to

$$\kappa_{2V} \in [-0.0, 2.1]\ ([-0.1, 2.1]),\quad \text{observed (expected) 95\% CL.} \tag{2.3}$$

The CMS Collaboration has also published results of a search for nonresonant $hh \to b\bar{b}b\bar{b}$ with its full Run 2 dataset [46], which restricts the allowed interval for κ_λ to $[-2.3, 9.4]$ ($[-5.0, 12.0]$), at 95% confidence level (CL). Furthermore, a more recent CMS publication [47] that exploits topologies arising from highly energetic Higgs boson decays into $b\bar{b}$, restricts the allowed interval for κ_{2V} to

$$\kappa_{2V} \in [0.62, 1.41]\ ([0.66, 1.37]),\ \text{at observed (expected) 95\% CL.} \tag{2.4}$$

ATLAS and CMS have conducted investigations into non-resonant hh in the $b\bar{b}\tau^+\tau^-$ [3–5, 8, 9] and $b\bar{b}\gamma\gamma$ [3, 6, 7] decay channels as well. In our analysis, we look at final state topologies for the highest di-Higgs branching ratios, i.e.,

$$pp \to hhjj \to b\bar{b}b\bar{b}jj, \tag{2.5a}$$

and,

$$pp \to hhjj \to b\bar{b}\tau^+\tau^- jj. \tag{2.5b}$$

We generate events for each process scanning over the space of κ_V and κ_{2V}, keeping $\kappa_\lambda = 1$ fixed, and perform a χ^2 fit to obtain the limits on the corresponding couplings.

2.1.1 Event generation and selection

To investigate WBF processes, we use MadGraph_aMC@NLO [41] with leading order precision at 13 TeV to generate our events and apply stringent cuts at the generator level on the WBF jet pair's invariant mass ($m_{jj} > 800$ GeV). Additionally, we set the pseudorapidity of the b-jets to be $|\eta_b| < 2.5$ to ensure that the b-jets produced from the Higgs pair are centrally located. We modify the MadGraph source code to include the κ modifiers for event generation. Subsequently, we shower the events with Pythia 8.3 [48] and use MadAnalysis [49] that interfaces FastJet [50, 51], to reconstruct the final state particles with a 70% b-tagging efficiency.

JHEP11(2023)158

Firstly, we define forward and central jets with the following selection criteria:

1. Forward jets: $p_T^j > 30$ GeV and $2.5 < |\eta_j| < 4.5$.
2. Central jets: $p_T^j > 40$ GeV and $|\eta_j| < 2.5$.

To select events in the $hh \to b\bar{b}b\bar{b}$ channel, we utilise the methodology described in [2]. Initially, we identify the jet pair with the highest invariant mass as the WBF jets and impose the forward-jet criteria on them. Next, we require at least 4 centrally located jets, all of which must be b-tagged. We also apply an additional pseudorapidity separation cut of $|\eta_{jj}| > 3$ and an invariant mass cut of $m_{jj} > 1$ TeV on the WBF-jets. To isolate the WBF region, we further demand that the transverse component of the momentum vector sum of the two WBF jets and the four jets forming the Higgs boson candidates be less than 65 GeV. The Higgs pair is constructed from the 4 b-jets and a minimum invariant mass of $M_{hh} > 400$ GeV is required.

For the $hh \to b\bar{b}\tau^+\tau^-$ channel, the WBF jet pair is chosen in the same manner as before, and we apply the same cuts on them. However, only two centrally located b-tagged jets are required in this case. The τ-leptons can decay either hadronically or leptonically, with the latter being selected using the criteria outlined in the latest ATLAS analysis [9], with a minimum p_T of 15 GeV and limited to $|\eta_l| < 2.47$. The light jets arising from the hadronic decay of the τ-leptons are selected with a minimum p_T of 10 GeV and $|\eta_j| < 2.5$. Additionally, the leptonic decay of the τ's results in missing energy. The di-Higgs invariant mass is then constructed using the two b-jets and the τ-decay products, with a minimum invariant mass requirement of $M_{hh} > 400$ GeV.

2.1.2 Sensitivity and projections

We use the distribution of the reconstructed kinematic observable M_{hh} to obtain the current and projected limits on the respective couplings. The χ^2 statistic for our analysis is computed as

$$\chi^2(\kappa_V, \kappa_{2V}) = (b^i_{\text{BSM}}(\kappa_V, \kappa_{2V}) - b^i_{\text{SM}}) V^{-1}_{ij} (b^j_{\text{BSM}}(\kappa_V, \kappa_{2V}) - b^j_{\text{SM}}), \tag{2.6a}$$

where $b^i_{\text{BSM}}(\kappa_V, \kappa_{2V})$ represents the combined number of events in the ith bin of M_{hh} from both decay channel, considering their respective cross-sections and efficiency, at a given luminosity for a particular value of κ_V and κ_{2V}, and b^i_{SM} corresponds to the expected number of events solely from the SM for $\kappa_V = 1$ and $\kappa_{2V} = 1$. The covariance matrix V_{ij} is the sum-in-quadrature of two terms: 1) the statistical uncertainties computed from the root of bin entries, i.e., the Poisson uncertainty associated with each bin, b^i_{SM}, and 2) fully correlated relative fractional uncertainties ($\varepsilon_{\text{rel.}}$), i.e.,

$$V_{ij} = b^i_{\text{SM}} \delta_{ij} + \varepsilon^2_{\text{rel.}} b^i_{\text{SM}} b^j_{\text{SM}} \,. \tag{2.6b}$$

To fix $\varepsilon_{\text{rel.}}$, we set $\kappa_V = 1$ and scan over κ_{2V} such that we reproduce a 95% CL limit of $\kappa_{2V} \in [0.2, 2.0]$ at $126\,\text{fb}^{-1}$ at the LHC, comparable to the limits set by ATLAS [2] and CMS [47].

JHEP11(2023)158

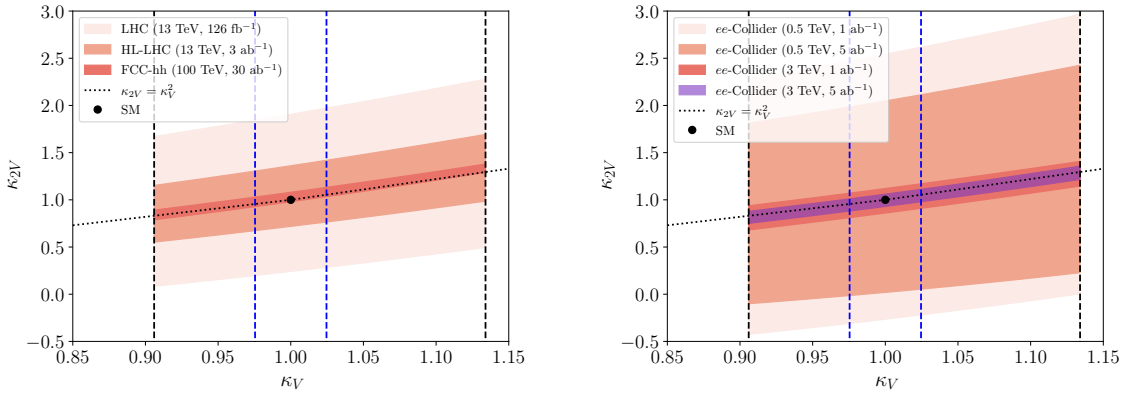

(a) (b)

Figure 3. Current and projected constraints on κ_V and κ_{2V} for various colliders. The current LHC and projected HL-LHC limits on κ_V, represented by the black and blue dashed lines respectively, have been set using Higgs data from ATLAS [55].

Once our methodology was validated through a comparison of our κ_{2V} constraints with the predictions of ATLAS (eq. (2.3)) and CMS (eq. (2.4)), we proceed to explore the parameter space of κ_V and κ_{2V} and obtain constraints at the 95% CL. Our results are presented in figure 3, where we show the 95% confidence bands for the LHC with an integrated luminosity of 126 fb^{-1}, the constraints for the High-Luminosity (HL-LHC) frontier with an integrated luminosity of 3 ab^{-1}, as well as the projected constraints for the Future Circular Collider (FCC-hh) with $\sqrt{s} = 100$ TeV and an integrated luminosity of 30 ab^{-1}, assuming the same $\varepsilon_{\text{rel.}}$ as for the LHC case. It should be added that using the χ^2 calibrated to [2, 47] is a conservative extrapolation for the FCC-hh. A limiting factor in this environment is the reduction of QCD multi-jet contributions as central jet vetoes are not available to suppress these efficiently. This can lead to a considerable variation of the expected sensitivity [52–54], in particular when considering the rejection of the irreducible gluon fusion component.

2.2 Lepton collider constraints on κ_V and κ_{2V}

The di-Higgs sector exploration at upcoming lepton colliders has garnered significant attention due to their exceptional sensitivity range, which is attributed to significantly lower background interference compared to hadron colliders. The works of [56–59] (see also refs. [60, 61]) have been instrumental in investigating the di-Higgs sector and obtaining exclusion limits on κ_λ and κ_V. Building on this success, we extend the scope of this exploration by attempting to obtain limits on κ_V and κ_{2V} for e^+e^--colliders, adopting a methodology similar to that presented in section 2.1. In this scenario, the di-Higgs decay into four b-quarks is very attractive since the background is orders of magnitude smaller, making it the primary focus of our analysis. The process we want to look at is, therefore,

$$e^+e^- \to hhe^+e^-/\nu_e\bar{\nu}_e \to b\bar{b}b\bar{b}e^+e^-/\nu_e\bar{\nu}_e. \tag{2.7}$$

JHEP11(2023)158

The dominant contributions to the production cross-section come from the WBF process and Higgs-strahlung. We generate our events with MadGraph for two benchmark collider beam energies of 0.5 TeV and 3 TeV. To select our WBF signal region, we closely follow the analysis in [56]. We firstly impose a strict missing energy cut greater than 30 GeV. Our study further requires four centrally located b-tagged jets, with $p_T > 20$ GeV and $|\eta| < 2.5$. In order to reconstruct the Higgses individually from the b's, we determine the labelling of the four b-jets, b_i, that minimises the quantity $(m_{12}/\text{GeV} - 125)^2 + (m_{34}/\text{GeV} - 125)^2$, where m_{ij} represents the invariant mass formed by jets b_i and b_j. We infer that b_1, b_2 come from one of the Higgs decay, and b_3, b_4 are the decay products of the other. We then demand that the corresponding jets reconstruct the two Higgs bosons within the on-shell window $(90\text{ GeV}, 130\text{ GeV})$.

With the selected signal events, we construct a χ^2 as described in section 2.1.2, again, scanning over κ_V and κ_{2V}. The constraints for both our benchmark points are presented in figure 3, at integrated luminosities of $\mathcal{L} = 1$ ab^{-1} and 5 ab^{-1}. Our analysis reproduces the CLIC projection [62],

$$\kappa_{2V} \in [0.97, 1.05], \text{ expected 95\% CL., 3 TeV, 5 ab}^{-1}. \tag{2.8}$$

However, the potential to exploit beam polarisations in [62] (which we do not, here in our comparison) indicates that our sensitivity estimates are conservative.

In the following sections, we will treat the κ_V single Higgs constraints independently from the $\kappa_{2V}, \kappa_\lambda$ constraints for presentation purposes (in our discussion below, these limits correspond to qualitatively different phenomenological parameters). Of course, the individual rectangular regions indicated in figure 3 are simultaneously constrained by these (correlated) data sets. To gauge how the rectangular regions map onto the elliptical constraints in a combination of this information for the most sensitive environments, we show a combination of single Higgs and weak boson fusion hh production in figure 4. This demonstrates that in particular at the very sensitive future collider environments that enable tight constraints on κ_{2V}, this parameter will remain less constrained compared to κ_V.

Remarks on κ_λ. Weak boson fusion processes at hadron colliders play a less relevant role in constraining Higgs self-interactions, predominantly the trilinear Higgs coupling, as Higgs pair production from gluon fusion $gg \to hh$ is more abundant. Representative extrapolations to the HL-LHC phase [64] indicate that this coupling could be constrained at 50% around its SM expectation. The environment of an FCC-hh at 100 TeV will increase the sensitivity to 3–5% [65].

Higgs self-coupling measurements at lepton colliders are dominated by Z-boson associated Higgs pair production for low centre-of-mass energies and WBF at large energies, e.g., at CLIC. The latter, maximising the WBF potential, has a projected sensitivity of about $\kappa_\lambda = 1^{+0.25}_{-0.15}$ with some level of degeneracy between κ_λ and κ_{2V} [62]. As for hadron colliders the constraint on κ_{2V} is stronger compared to κ_λ which highlights the need for constraining κ_λ at hadron colliders such as the LHC. The sensitivity at CLIC compares to an estimated ILC sensitivity (in the 250 GeV+500 GeV combined phase) of $\kappa_\lambda = 1 \pm 0.25$ [66].

JHEP11(2023)158

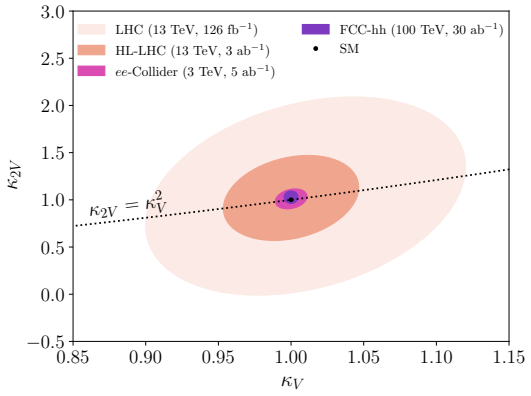

Figure 4. The 95% CL constraints on κ_V and κ_{2V} parameter space resulting from the combination of WBF di-Higgs and single Higgs production for various collider options. Single Higgs constraints for future colliders are taken from the κ_W bounds in [63].

The main focus of our work is a discussion of κ_{2V}, κ_V in WBF as this channel is primarily sensitive to these parameters due to eq. (2.2). We will include, however, details on κ_λ and its relevance in comparison to κ_{2V}, κ_V in the discussion of the next section 3. κ_λ is known to be relatively efficiently constrainable in gluon fusion Higgs pair production through sensitivity in the threshold region, whose inclusive cross section [67, 68] is an order of magnitude larger than WBF. Our discussion of κ_λ should therefore be understood as a potential additional constraint when considering κ_{2V} measurements as performed by the experiments.

3 κ_V, κ_{2V} and κ_λ in BSM models

In this section, we consider how different BSM models populate the space of κ_V, κ_{2V}, and κ_λ. We pay particular attention to those models that predict order-of-magnitude larger deviations in either κ_{2V} or κ_λ relative to κ_V; in such cases future measurements of either κ_{2V} or κ_λ are likely to provide significant discriminating power. As discussed recently in [69], and as we elucidate below, a large deviation in κ_{2V} relative to κ_V will require non-decoupling TeV scale new physics.

3.1 Extended scalar sectors, tree level

Consider a generic extended scalar sector, built out of a set M of electroweak multiplets Φ_A. Let Φ_A have an SU(2) irreducible representation (irrep) of dimension d_A, and a hypercharge Y_A, with renormalisable lagrangian

$$\mathcal{L} = \sum_{A \in M} |D\Phi_A|^2 - V(\Phi)\,. \tag{3.1}$$

We define the charged current part of the covariant derivative to be

$$D_\mu \Phi_A = \left(\partial_\mu - \frac{1}{\sqrt{2}} i g_W (W_\mu^+ T_A^+ + W_\mu^- T_A^-) - \dots\right) \Phi_A\,, \tag{3.2}$$

JHEP11(2023)158

where the components of the generators in the SU(2) irrep of dimension d_A are given by

$$[T_A^{\pm}]_{\alpha\beta} = \begin{cases} \sqrt{\left(\frac{d_A+1}{2}\right)(\alpha+\beta-1)-\alpha\beta} & \text{if } \alpha \pm 1 = \beta \\ 0 & \text{otherwise} \end{cases}, \tag{3.3}$$

with the SU(2) indices α, β running between 1 (labelling the component with maximum third component of isospin, T^3) and d_A (labelling the component with minimum T^3).

The $\left[\left(\frac{d_A+1}{2}\right)+Y_A\right]$-th component is electrically neutral, and after electroweak symmetry breaking can be decomposed into vevs, v_R and v_I, and vev-free fields h_R and h_I

$$[\Phi_A]_{\left(\frac{d_A+1}{2}\right)+Y_A} = \frac{1}{\sqrt{2}}(v_R+h_R)+\frac{i}{\sqrt{2}}(v_I+h_I)\,. \tag{3.4}$$

These are separated into real (R) and imaginary (I) parts. The imaginary components are absent from real irreps, as well as, without loss of generality, from one complex irrep due to our freedom to gauge it away. Assuming the scalar sector contains a hypercharge-$\frac{1}{2}$ doublet, we gauge away its imaginary component.

Substituting eqs. (3.2) and (3.4) into eq. (3.1) we see that in the broken phase the charged current interactions of the neutral Higgses are governed by

$$\mathcal{L} = \sum_i \frac{1}{2}(\partial h_i)^2 - V(v,h) + \frac{1}{4}g_W^2 W^+W^- \left[C_{ij}v_iv_j + 2C_{ij}v_ih_j + C_{ij}h_ih_j\right] + \dots\,, \tag{3.5}$$

where i, j index the neutral Higgses, and repeated indices are summed over, and the matrix C is diagonal with entries

$$C_{ij} = \delta_{ij}\left(\frac{1}{2}(d_A^2-1)-2Y_A^2\right)\,. \tag{3.6}$$

d_A, Y_A are the dimension and hypercharge of the multiplet from which the ith component came: real and imaginary components of the same multiplet have the same entry. C_{ij} is normalised to be the identity matrix in an n-Higgs doublet model.

The 125 GeV Higgs, h, is defined as a unit direction in the space of neutral Higgs components:

$$h_i = h\,\hat{n}_i\,,\ \text{where } \hat{n}_i\hat{n}_i = 1\,. \tag{3.7}$$

We substitute the above into eq. (3.5) and compare with eq. (2.1). Identifying the total vev as

$$v \equiv (C_{ij}v_iv_j)^{\frac{1}{2}} = 246\,\text{GeV}\,, \tag{3.8}$$

we obtain the coupling modifiers

$$\begin{aligned} \kappa_V &= \frac{C_{ij}v_i\hat{n}_j}{(C_{ij}v_iv_j)^{\frac{1}{2}}}\,, \\ \kappa_{2V} &= C_{ij}\hat{n}_i\hat{n}_j\,. \end{aligned} \tag{3.9}$$

Note that we have assumed the electroweak multiplets form complete custodial irreps, so that $\kappa_V = \kappa_W = \kappa_Z$ and $\kappa_{2V} = \kappa_{2W} = \kappa_{2Z}$.

JHEP11(2023)158

κ_V and κ_{2V} are therefore correlated in particular extended scalar sectors, i.e. for particular C_{ij}. We give the examples of the singlet, second Higgs doublet, and Georgi-Machacek model in table 2 and appendix A. In figure 7, we show the lines and regions that these models can populate in the κ_V-κ_{2V} plane. Notably, for *any* tree-level model

$$v^2\left(\kappa_{2V}-\kappa_V^2\right) = C_{ij}\hat{n}_i\hat{n}_j\, C_{kl}v_k v_l - (C_{ij}v_i\hat{n}_j)^2 \geq 0\,, \tag{3.10}$$

which follows from the Cauchy-Schwartz inequality when C is a positive definite matrix. It is only zero in the alignment limit, when $\hat{n}_i \propto v_i$, or in the case of mixing with singlets, when C is only positive semidefinite.

Thus, to obtain a large deviation in κ_{2V} but not κ_V in an extended scalar sector, we require electroweak triplets or higher representations, and a departure from the alignment limit (i.e., a departure from the parabola $\kappa_{2V} = \kappa_V^2$), see also [70]. This in turn implies significant mixing of components of the Higgs doublet with other states that cannot be made arbitrarily heavy. This is likely to cause some tension with direct searches. For instance, a significant triplet component to electroweak symmetry breaking introduces resonant tell-tale same-sign WW WBF production [71] which drives constraints on the triplet nature of the observed Higgs boson [72] (see also [73]). Finally, we remark here that, in the decoupling limit, both κ_V and κ_{2V} approach 1, and in principle do so from different directions in the κ_V-κ_{2V} plane, depending on the model — compare, for instance, the singlet and 2HDM trajectories in figure 7. However, in the decoupling limit, the deviations from the Standard Model in $WW \to hh$ due to κ_V, κ_{2V} are comparable to the short-distance contributions from heavy Higgs exchange. These latter exchange contributions are calculated for the singlet and 2HDM model in [74], where this effect is discussed in detail. The effect of both κ_{2V} and the short distance heavy Higgs exchange can be combined into a κ_{2V}^{eff}, which satisfies

$$1-\kappa_V^2 = \kappa_V^2 - \kappa_{2V}^{\text{eff}}\,, \tag{3.11}$$

in the decoupling limit. This corresponds to the pattern predicted by the SMEFT at dimension 6 (see, e.g., [69]).

Turning now to κ_λ, this is generally a free parameter for renormalisable potentials $V(\Phi)$ containing cubic interactions among the electroweak irreps. However, if the cubic interactions are absent (as often happens accidentally due to the charges of the multiplets, or is imposed by certain $\mathbb{Z}_2$ symmetries), we can begin to understand the range of κ_λ close to the alignment limit. The potential among the neutral components before electroweak symmetry breaking will have the generic form

$$V = \frac{1}{2}\mu_{ij}^2 r_i r_j + \frac{1}{4}\lambda_{ijkl} r_i r_j r_k r_l\,, \tag{3.12}$$

where the tensors μ^2 and λ are necessarily symmetric in their indices, and $r_i = 0$ corresponds to the electroweak symmetry preserving vacuum. After electroweak symmetry breaking, substituting $r_i = v_i + h_i$ leads to

$$V = \text{const.} + \frac{1}{2}\mu_{ij}^2 h_i h_j + \frac{3}{2}\lambda_{ijkl} h_i h_j v_k v_l + \lambda_{ijkl} h_i h_j h_k v_l + \mathrm{O}(h^4) \tag{3.13}$$

JHEP11(2023)158

where we've used the vev condition

$$\mu_{ij}^2 v_j + \lambda_{ijkl} v_j v_k v_l = 0\,. \tag{3.14}$$

From comparison with eq. (2.1), κ_λ takes the form

$$\kappa_\lambda = (C_{ij} v_i v_j)^{\frac{1}{2}} \frac{2\lambda_{ijkl}\hat{n}_i\hat{n}_j\hat{n}_k v_l}{m_h^2} \tag{3.15}$$

Close to the alignment limit, eq. (3.15) can be expressed in terms of mass parameters and the degree of alignment. We work, without loss of generality, in the mass basis where the mass matrix of eq. (3.13) satisfies

$$\begin{aligned} \mu_{11}^2 + 3\lambda_{11kl} v_k v_l &= m_h^2 \\ \mu_{1a}^2 + 3\lambda_{1akl} v_k v_l &= 0 \\ \mu_{ab}^2 + 3\lambda_{abkl} v_k v_l &= m_a^2 \delta_{ab} \end{aligned} \tag{3.16}$$

where $a, b = 2, 3, \ldots$ label heavy Higgs directions, each with mass m_a^2. In this basis, v_i satisfies

$$v_i = v\left(1 - \frac{1}{2}\epsilon_a\epsilon_a,\, \epsilon_2,\, \epsilon_3, \ldots\right)^T + \mathrm{O}(\epsilon^3)\,, \tag{3.17}$$

for some small parameters ϵ_a describing the amount of the vev in the heavy Higgs directions when close to the alignment limit. Summation is implied over repeated a indices.

Expanding $\mu_{11}^2, \mu_{1a}^2, \mu_{ab}^2$ and $\lambda_{111l} v_l, \lambda_{11al} v_l, \lambda_{1abl} v_l$ order-by-order in ϵ_a, eqs. (3.14) and (3.16) can be expanded to solve for

$$\kappa_\lambda = \frac{2v\lambda_{111l} v_l}{m_h^2} = 1 + \frac{1}{2}\epsilon_a\epsilon_a - 2\epsilon_a\epsilon_b \frac{(\lim_{\epsilon_a \to 0} \mu_{ab}^2)}{m_h^2} + \mathrm{O}(\epsilon^3)\,. \tag{3.18}$$

In the decoupling limit, where m_a^2 are large, the model is necessarily aligned and $\epsilon_a \sim \mathrm{O}\left(\frac{1}{m_a^2}\right)$ are correspondingly small. The quartic couplings of the model are limited in size by perturbative unitarity, and so from eq. (3.16) μ_{ab}^2 approaches $m_a^2\delta_{ab}$. In this case

$$\kappa_\lambda \approx 1 - 2\sum_a \epsilon_a^2 \left(\frac{m_a^2}{m_h^2} - \frac{1}{4}\right)\,, \tag{3.19}$$

and the deviation in κ_λ enjoys a parametric enhancement of $\frac{m_a^2}{m_h^2}$ relative to the deviations in κ_V^2 and κ_{2V} which are both $\mathrm{O}(C \times \epsilon_a^2)$. We note that this enhancement does not necessarily happen in the case of *alignment without decoupling*.

3.2 Extended scalar sectors, loop level

We turn to the case of an arbitrary electroweak scalar multiplet, Φ_A, with a $\mathbb{Z}_2$ symmetry that prevents it from acquiring a vev, and a cross quartic interaction λ with the SM Higgs doublet Φ:

$$\mathcal{L} = |D\Phi_A|^2 - m_\varphi^2 |\Phi_A|^2 - 2\lambda |\Phi_A|^2 \left(\Phi^\dagger\Phi - \frac{v^2}{2}\right)\,. \tag{3.20}$$

JHEP11(2023)158

If the scalar is sufficiently heavy, $2m_\varphi > m_h$, its leading order effects are at one-loop level. When augmented with a small amount of $\mathbb{Z}_2$ splitting to allow charged particles to decay, eq. (3.20) presents a minimal class of models that includes multiple viable candidates for BSM particles of mass $m_\varphi^2 \lesssim 1\,\text{TeV}$ [75]. If the cross quartic is large, such that $m_\varphi^2 \sim \lambda v^2$, sizeable effects in the electroweak phase transition are expected [76].

In the simplest case of a $\mathbb{Z}_2$ symmetric singlet, $\sqrt{2}\Phi_A \sim \sqrt{2}\Phi_A^\dagger \sim S$ and eq. (3.20) reads

$$\mathcal{L} = \mathcal{L}_{\text{SM}} + \frac{1}{2}(\partial_\mu S)^2 - \frac{m_S^2}{2}S^2 - \lambda S^2\left(\Phi^\dagger\Phi - \frac{v^2}{2}\right). \tag{3.21}$$

In this scenario the $WW \to hh$ subamplitudes (as any amplitude) can be renormalised. We adopt the on-shell scheme as described in ref. [77], which is the common scheme used for electroweak corrections (we are treating tadpoles as parameters as in ref. [78]).[3] The effects of the singlet, to order $\mathrm{O}(\lambda^3)$, can be accounted for by substituting the following finite expressions into figure 1

$$\begin{aligned}
\kappa_{2V} - 1 &= -\frac{\lambda^2 v^2}{8\pi^2}\text{Re}\left[B_0'(m_h^2, m_S^2, m_S^2)\right] \simeq \kappa_V^2 - 1\,, \\
\kappa_\lambda - 1 &= -\frac{\lambda^3 v^4}{6\pi^2 m_h^2}C_0(M_{hh}^2, m_h^2, m_S^2) \\
&\quad - \frac{\lambda^2 v^2}{8\pi^2}\frac{1}{M_{hh}^2 - m_h^2}\left(B_0(M_{hh}^2, m_S^2, m_S^2) - \text{Re}[B_0(m_h^2, m_S^2, m_S^2)]\right) \\
&\quad - \frac{\lambda^2 v^2}{48\pi^2 m_h^2}(4B_0(m_h^2, m_S^2, m_S^2) + 2B_0(M_{hh}^2, m_S^2, m_S^2) \\
&\qquad\qquad - \text{Re}[6B_0(m_h^2, m_S^2, m_S^2) - 3m_h^2 B_0'(m_h^2, m_S^2, m_S^2)])\,.
\end{aligned} \tag{3.22}$$

Here B_0, B_0' are the Passarino-Veltman [80] two-point function and its derivative, respectively, and C_0 is the 3-point function. κ_λ becomes an M_{hh}^2-dependent form factor; this momentum dependence is particularly useful for light scalar masses m_S which do not admit a reliable EFT description and can modify the phenomenology at threshold.

Note that, for the loop-level singlet, the correction to κ_V and κ_{2V} is purely through the wavefunction renormalisation of the Higgs, and therefore follows a characteristic $\kappa_V^2 \simeq \kappa_{2V}$ pattern, the corrections to both scaling as λ^2. κ_λ, on the other hand, receives a λ^3 contribution from a 1PI singlet loop. When λ is large, this generically means the κ_λ sensitivity to this model at HL-LHC is greater than that of κ_V, κ_{2V}, as illustrated in figure 5.

In principle, a Φ_A with non-trivial electroweak charges can contribute 1PI corrections to hWW and $hhWW$ vertices; in practice, however, these states' corrections to the κ parameters are parametrically similar to the singlet case. To see this, take Φ_A to be a second (inert) Higgs doublet as a representative example, and work to order $\mathrm{O}(m_\varphi^{-2})$, assuming the extra states are sufficiently heavy for their effects in $WW \to hh$ to be well approximated by constant κs. Performing the same calculation as before in the on-shell

[3] Specifically, we choose $\{m_W, m_Z, \alpha\}$ as input parameters for the electroweak sector. The Weinberg angle is then a derived quantity [79].

JHEP11(2023)158

scheme we obtain, for the off-shell SM-like 1 particle irreducible vertex functions Γ,

$$\begin{aligned}
\left.\frac{\Gamma^{WWh}}{\Gamma^{WWh}_{\rm LO}}\right|_{\rm SM} &= \bar\kappa_W = 1 - \frac{g_W^2}{1920\pi^2 m_\varphi^2}\left(2m_W^2 + m_Z^2\right) - \frac{\lambda^2 v^2}{24\pi^2 m_\varphi^2}\,,\\
\left.\frac{\Gamma^{WWh}}{\Gamma^{WWh}_{\rm LO}}\right|_{\rm SM} &= \bar\kappa_Z = \bar\kappa_W + \frac{g_Y^2}{960\pi^2 m_\varphi^2}(m_W^2 - m_Z^2)\,,\\
\left.\frac{\Gamma^{WWhh}}{\Gamma^{WWhh}_{\rm LO}}\right|_{\rm SM} &= \bar\kappa_{2W} = 1 - \frac{g_W^2}{480\pi^2 m_\varphi^2}\frac{c_W^2}{s_W^2}\left(m_W^2 + m_Z^2\right) - \frac{\lambda^2 v^2}{12\pi^2 m_\varphi^2}\,,\\
\left.\frac{\Gamma^{ZZhh}}{\Gamma^{ZZhh}_{\rm LO}}\right|_{\rm SM} &= \bar\kappa_{2Z} = \bar\kappa_{2W} + \frac{e^4 v^2}{1920\pi^2 m_\varphi^2}\frac{g_Y^2}{g_W^2}\,,\\
\left.\frac{\Gamma^{hhh}}{\Gamma^{hhh}_{\rm LO}}\right|_{\rm SM} &= \bar\kappa_\lambda = 1 - \frac{g_W^2 m_Z^2}{1920\pi^2 m_\varphi^2} - \frac{\lambda^2 v^2}{72\pi^2 m_\varphi^2}\left(7 + 2\frac{M_{hh}^2}{m_h^2}\right) + \frac{\lambda^3 v^2}{3\pi^2 m_\varphi^2}\frac{v^2}{m_h^2}\,.
\end{aligned} \tag{3.23}$$

We highlight the fact that these are no longer related to physical quantities by introducing the bar. The physical couplings in the amplitudes are the product of both these corrections to the κs, and the corrections to the electroweak couplings due to the non-trivial gauge quantum numbers of the new fields. In particular, for non-vanishing hypercharge, the new states are additional sources of custodial isospin violation as directly visible above. The gaugeless part of the corrections mirrors those of the singlet eq. (3.22). In particular, the $\mathrm{O}(\lambda^2)$ corrections to κ_V and κ_{2V} come exclusively from wavefunction normalisation of the Higgs boson.[4]

The above results clearly show that additional gauge interactions can sculpt the κ_V, κ_{2V} parameter regions, however in a phenomenologically highly suppressed way compared to new additional inter-scalar interactions. Focussing on the gauge-independent part in practical $\kappa_{2V}, \kappa_V, \kappa_\lambda$ analyses, the λ contributions all scale with the number of real degrees of freedom, D. This gives approximate values for an arbitrary irrep of

$$\begin{aligned}
\kappa_V \simeq \bar\kappa_V &\approx 1 - D\,\frac{\lambda^2 v^2}{96\pi^2 m_\varphi^2}\,,\\
\kappa_{2V} \simeq \bar\kappa_{2V} &\approx 1 - D\,\frac{\lambda^2 v^2}{48\pi^2 m_\varphi^2}\,,\\
\kappa_\lambda \simeq \bar\kappa_\lambda &\approx 1 + D\,\frac{\lambda^3 v^2}{12\pi^2 m_\varphi^2}\frac{v^2}{m_h^2}\,.
\end{aligned} \tag{3.24}$$

where we have assumed $\lambda v^2 \gg m_h^2$ to drop the λ^2 piece in κ_λ, and focused on the HL-LHC measurement region $M_{hh} \gtrsim 2m_h$. The full momentum dependence for any such irrep can be restored from eq. (3.22) by multiplying by the dimension D.

3.3 From compositeness to dilaton mixing

The κ values of a composite Higgs model depend on the details of the symmetry breaking. In the minimal composite Higgs model (MCHM), the components of the Higgs doublet

[4] Parametrically comparable 1PI contributions to HWW and $HHWW$ arise from dimension-six operators $\sim |\Phi|^2 V_\mu V^\mu$. In cases where couplings are forbidden by gauge-invariance, eq. (1.1), the dimension-6 contributions are conventionally included to the κ definition as is the case for $\kappa_\gamma, \kappa_g, \kappa_{Z\gamma}$, see e.g. [81, 82].

JHEP11(2023)158

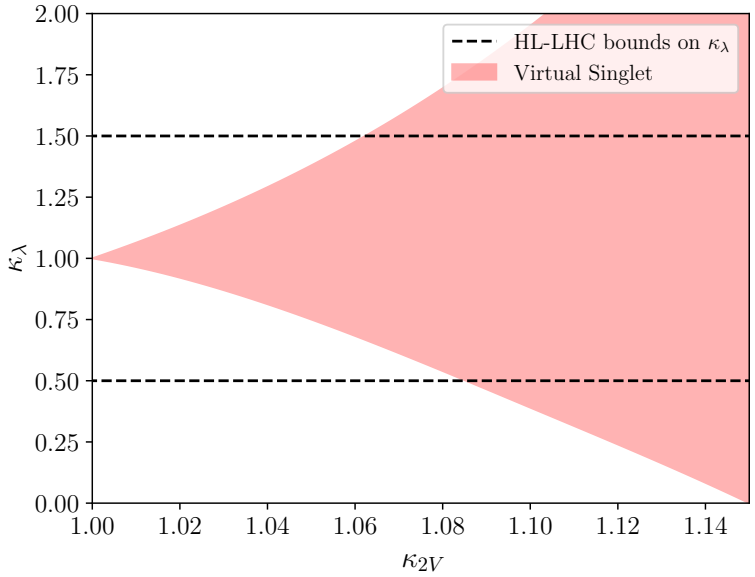

Figure 5. κ_λ-κ_{2V} plot for the aforementioned singlet mixing scenario for a representative value of $M_{hh} = 300$ GeV $\gtrsim 2m_h$ which provides the region sensitive to κ_λ investigations in Higgs pair production from gluon fusion. The HL-LHC projected sensitivity bounds on κ_λ is represented by the dashed black lines [64]. The range on the κ_{2V} axis comes from HL-LHC bounds on κ_V, assuming $\kappa_{2V} = \kappa_V^2$ as in this singlet model. We vary $m_S \in [90, 400]$ GeV and $\lambda \in [-2, 2]$ to obtain the contour.

chart the coset SO(5)/SO(4) [16, 17, 83], whose relevant dynamics are readily constructed through the linear sigma model, see [84]. The five components $\phi^1, \ldots, \phi^5$ have kinetic terms

$$\mathcal{L} = \frac{1}{2}\sum_{M=1}^{4}\left((D\phi)^M\right)^2 + \frac{1}{2}(\partial\phi^5)^2\,, \tag{3.25}$$

where the first four components have SM-like gauge couplings to the W and Z. The components are restricted to the surface

$$\sum_{M=1}^{4}(\phi^M)^2 + (\phi^5)^2 = f^2 \tag{3.26}$$

which, in unitary gauge, can be parametrised by

$$\left(\phi^1, \phi^2, \phi^3, \phi^4, \phi^5\right) = \left(0, 0, 0, f\sin\frac{\mathfrak{h}}{f}, f\cos\frac{\mathfrak{h}}{f}\right) \tag{3.27}$$

where $\mathfrak{h}$ is understood to be the Higgs coordinate shifted such that $\mathfrak{h} = 0$ in the absence of electroweak symmetry breaking. Substitution of eq. (3.27) into eq. (3.25) yields the unitary gauge lagrangian

$$\mathcal{L} = \frac{1}{2}(\partial\mathfrak{h})^2 + \frac{g_W^2 f^2}{4}\sin^2\left(\frac{\mathfrak{h}}{f}\right)\left[W^+W^- + \frac{1}{2c_W^2}Z^2\right]\,, \tag{3.28}$$

JHEP11(2023)158

and expanding about the vacuum $\mathfrak{h} = \langle \mathfrak{h} \rangle + h$ then gives

$$\begin{aligned} \kappa_V &= \sqrt{1-\xi}\,, \\ \kappa_{2V} &= 1 - 2\xi\,, \end{aligned} \tag{3.29}$$

in terms of $\xi = \frac{v^2}{f^2}$. While this pattern will change for different cosets, it was shown in [85] that for all custodial-symmetry-preserving cosets arising from the breaking of a compact group, it is guaranteed that

$$\begin{aligned} 1 - \kappa_V^2 &\geq 0\,, \\ \kappa_V^2 - \kappa_{2V} &\geq 0\,. \end{aligned} \tag{3.30}$$

By contrast, this can be violated for non-compact groups. A non-compact coset $\mathrm{SO}(4,1)/\mathrm{SO}(4)$ can be constructed via the linear sigma model lagrangian [84]

$$\mathcal{L} = \frac{1}{2}\sum_{M=1}^{4}\left((D\phi)^M\right)^2 - \frac{1}{2}(\partial\phi^5)^2\,, \tag{3.31}$$

restricted to the surface

$$\sum_{M=1}^{4}(\phi^M)^2 - (\phi^5)^2 = -f^2 \tag{3.32}$$

which is parametrised in unitary gauge by

$$\left(\phi^1, \phi^2, \phi^3, \phi^4, \phi^5\right) = \left(0, 0, 0, f\sinh\frac{\mathfrak{h}}{f}, f\cosh\frac{\mathfrak{h}}{f}\right)\,. \tag{3.33}$$

(Note that trigonometric functions in eq. (3.27) become hyperbolic ones in eq. (3.33), similar in spirit to the compactification of the Lorentz group.) This yields

$$\begin{aligned} \kappa_V &= \sqrt{1+\xi}\,, \\ \kappa_{2V} &= 1 + 2\xi\,, \end{aligned} \tag{3.34}$$

for the hyperbolic composite Higgs model.

In composite Higgs theories, the Higgs potential can be written schematically in MCHM5 (and MCHM5-like theories such as ref. [86], where the 5 refers to the spurionic irrep of the top quark) as

$$f^{-4}V_{\mathrm{CH}}\left(\frac{\mathfrak{h}}{f}\right) = \alpha\cos\left(\frac{2\mathfrak{h}}{f}\right) - \beta\sin^2\left(\frac{2\mathfrak{h}}{f}\right) = \frac{m_H^2}{8v^2(1-\xi)}\left[\sin^2\left(\frac{\mathfrak{h}}{f}\right) - \xi\right]^2 + V_0\,, \tag{3.35}$$

where V_0 is a constant, see also [87]. The coefficients α, β are related to two and four-point functions of the underlying strongly interacting theory [88, 89] responsible for partial compositeness, and they can be replaced as a function of ξ and the Higgs mass. These coefficients can in principle be inferred from lattice computations (for recent progress see [90, 91]) to uncover realistic UV completions. The Higgs trilinear coupling modifier is then given by

$$\kappa_\lambda = \frac{1-2\xi}{\sqrt{1-\xi}} \tag{3.36}$$

JHEP11(2023)158

The expression for the hyperbolic composite Higgs model is again obtained from the replacement $\xi \to -\xi$ [84].

We note that the above expressions satisfy

$$\kappa_V \kappa_\lambda = \kappa_{2V} \,. \tag{3.37}$$

Therefore figure 1(a) reproduces the behaviour of figure 1(b) at leading order in the MCHM5 scenario. This is due to the symmetry breaking potential being of the same functional form as the interaction of the Goldstone bosons.[5]

Ultimately, the value of κ_λ depends on the (spurionic) representations of the explicit SO(4) symmetry breaking in the model. Larger representations, leading to higher order Gegenbauer polynomials of $\sin\left(\frac{h}{f}\right)$ in the potential, can break the above correlation between κ_λ and κ_V, κ_{2V}, and generally lead to a parametric enhancement in the deviations of κ_λ from the Standard Model [93].

3.3.1 Deforming the MCHM with a dilaton

The MCHM, together with its hyperbolic counterpart, define a line in the κ_V-κ_{2V} plane (shown in green and blue in figure 6) corresponding to the maximally symmetric coset spaces of constant positive or negative curvature [94]. Reference [69] considered deformations away from this line that can arise from deformations of the coset space. Here, we begin similarly, and argue that a viable model for these deformations comes from mixing of the composite Higgs with a TeV scale dilaton.

Practically, the coset space can be deformed by replacing the constant radius f in eqs. (3.26) and (3.32) with a mildly ϕ^5 dependent function

$$f^2 \to f^2(\phi^5) \approx f_0^2 + f_0^2 \frac{(\phi^5)^2}{f_t^2} \,, \tag{3.38}$$

for some $f_t^2 > f_0^2$. This promotes ϕ^5 to a modulus that is common in higher dimensional theories of electroweak symmetry breaking.[6] We calculate the modifications κ_V, κ_{2V} to linear order in f_0^2/f_t^2, after performing a field redefinition to canonically normalise the kinetic terms. (This field redefinition necessarily introduces momentum-dependent self-interactions of the would-be Higgs boson, to which we return below.) Scanning over f_0^2/f_t^2, we see from figure 6 that such manifolds deviate from the line of uniform curvature in the κ_V-κ_{2V} plane.

The effective ϕ^5 dependence of f can be brought about through mixing with a dilaton direction, χ, which we analyse here using the approach of [96]. χ measures the departure from conformal symmetry through its vacuum expectation value $\langle\chi\rangle$ [97]. In a UV completion where the composite Higgs components are mesonic states arising from a confining gauge

[5] In MCHM4 the potential reads $f^{-4}V_{\rm CH}\left(\frac{h}{f}\right) = \alpha\cos\left(\frac{h}{f}\right) - \beta\sin^2\left(\frac{h}{f}\right)$ leading to $\kappa_\lambda = \sqrt{1-\xi}$, see also [92]. In this scenario, which suffers from tension with electroweak precision constraints, we also have $\kappa_V\kappa_\lambda \neq \kappa_{2V}$.

[6] The motivation of the scalar metric from which this theory derives also follows the discussion presented in [95]. We have expanded to order $(\phi^5)^2$, assuming the linear term is forbidden by symmetry, so a linear deformation will not change our findings qualitatively.

JHEP11(2023)158

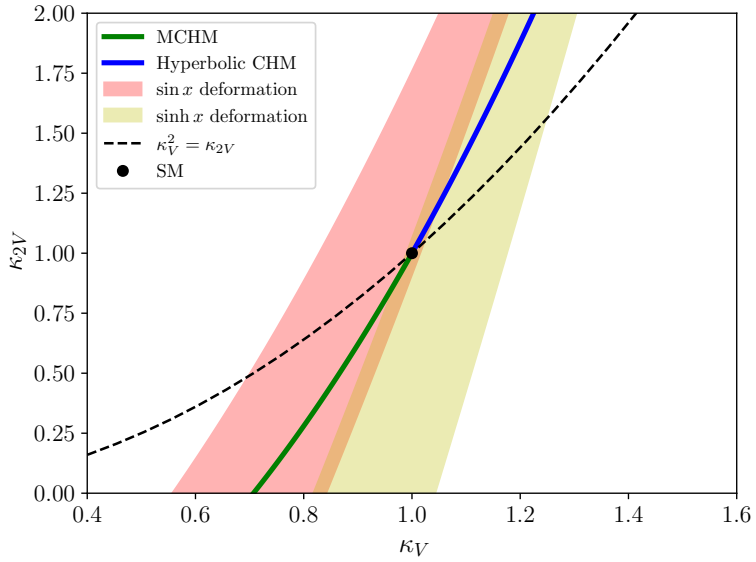

Figure 6. κ_V-κ_{2V} predictions for the composite Higgs models and their deformation through eq. (3.38) as described in the text. We scan $\kappa_V \in [0.5, 1.5]$, $\xi = v^2/f^2 \in [0, 1]$, and f_t as a consistent solution of the W mass given κ_V, ξ. This leaves κ_{2V} determined as a function of these parameters.

group SU(N_c), $\langle\chi\rangle \sim f$ if the dilaton is another mesonic state, $\langle\chi\rangle \sim f\sqrt{N_c}$ if the dilaton is a glueball like state [96]. Here $\langle\chi\rangle$ is a free parameter, which we require to be O(TeV) in order to get sizeable mixing effects with the composite Higgs states.

Interaction terms with the composite Higgs can be constructed by multiplying operators by $(\chi/\langle\chi\rangle)^n$, where n is the canonical mass dimension of the operator, in order to restore conformal symmetry. Thus

$$\mathcal{L} \supset \frac{g_W^2 f^2}{4}\left(\frac{\chi}{\langle\chi\rangle}\right)^2 \sin^2\left(\frac{\mathfrak{h}}{f}\right)\left[W^+W^- + \frac{1}{2c_W^2}Z^2\right] - \left(\frac{\chi}{\langle\chi\rangle}\right)^4 V_{\rm CH}\left(\frac{\mathfrak{h}}{f}\right), \tag{3.39}$$

in terms of the composite Higgs model operators eqs. (3.28) and (3.35). Expanding this lagrangian around the minimum $\langle\mathfrak{h}\rangle, \langle\chi\rangle$ and including effects of Higgs-dilaton mixing through the usual isometry

$$\begin{pmatrix} h \\ \chi - \langle\chi\rangle \end{pmatrix} = \begin{pmatrix} c_\phi & s_\phi \\ -s_\phi & c_\phi \end{pmatrix}\begin{pmatrix} h' \\ \chi' \end{pmatrix}, \tag{3.40}$$

we obtain, from the couplings of the mass eigenstate h',

$$\begin{aligned} \kappa_V &= c_\phi\sqrt{1-\xi} - s_\phi\sqrt{\zeta}\,, \\ \kappa_{2V} &= (1-2\xi)c_\phi^2 + \zeta s_\phi^2 - 2\sqrt{\zeta(1-\xi)}s_{2\phi}\,, \\ \kappa_\lambda &= c_\phi^3\frac{1-2\xi}{\sqrt{1-\xi}} - 4c_\phi^2 s_\phi\sqrt{\zeta} - 8\frac{V_0}{m_h^2 v^2}s_\phi^3\zeta^{\frac{3}{2}}\,, \end{aligned} \tag{3.41}$$

where $\zeta = v^2/\langle\chi\rangle^2$, and we have taken the MCHM5 potential for $V_{\rm CH}$ from eq. (3.35).

These couplings indeed cover, a priori, a wide area in the κ_V-κ_{2V} plane. In particular, the area $\kappa_{2V} < 1 < \kappa_V$, which was not populated by the models considered in previous

JHEP11(2023)158

sections, can be reached if the Higgs is considered mostly as a pseudo-dilaton. This area partially overlaps with the geometric deformations shown in figure 6 (eq. (3.38) can be thought of as approximating the leading order effects of dilaton mixing).

κ_λ can also accommodate large deviations from 1 in the case of significant Higgs-dilaton mixing. In addition, the dilaton χ has additional χ^3 terms from explicit sources of conformal symmetry violation as described in [97, 98]. This means that trilinear interactions will receive momentum-dependent interactions as a consequence of the a-theorem [99] leading to

$$\mathcal{L} \supset \frac{4\,\Delta a}{\langle\chi\rangle^3}\,(\partial\chi)^2\,\Box\,\chi + \dots \tag{3.42}$$

where the ellipses denote higher order terms in the dilaton and $\Delta a = \mathrm{O}(\%)$ (see [99, 100]). This leads to an additional momentum-dependent modifications of κ_λ of

$$\Delta\kappa_\lambda = s_\phi^3 \frac{4\,\Delta a}{3}\,\zeta\,\left[\frac{M_{hh}}{\langle\chi\rangle}\right]^2\,\left[\frac{M_{hh}}{m_h}\right]^2\,\left(1-\frac{4m_h^2}{M_{hh}^2}\right)\,, \tag{3.43}$$

with M_{hh} denoting the invariant di-Higgs mass. Modifications vanish close to the threshold, but can lead to a large modification of the invariant di-Higgs mass spectrum for considerable mixing.

The examples discussed so far exhaust the phenomenological possibilities in the κ_V-κ_{2V} plane, and therefore provide a theoretical avenue to interpret the results of associated analyses. Of course, κ_V constraints are also informed by single Higgs measurements and therefore there are significant constraints on these scenarios from a range of experimental findings. Similarly, both momentum-dependent and momentum-independent modifications to κ_λ are best constrained in measurements of gluon fusion Higgs pair production, given the larger rate and the generic sensitivity of WBF to (multi-) gauge boson interactions.

3.4 Running of coupling modifiers

Going beyond tree level, the correlations of κ_V, κ_{2V}, and κ_λ become scale and scheme dependent. In the Higgs effective field theory, the leading-order operators that modify κ_V, κ_{2V}, and κ_λ (free, uncorrelated parameters in HEFT) not only run into each other, but also into higher derivative, next-to-leading-order operators that modify the measured κs, as shown in table 1. To encapsulate these effects, we define an effective κ_V from the coefficient of $g^{\mu\nu}$ in the effective vertex for hWW (as defined in [15, 101])

$$Z_h^{\frac{1}{2}}\hat{\Gamma}^{\mu\nu}_{HW^-W^+}\,, \tag{3.44}$$

with all legs on shell. The wavefunction normalisation of the Higgs is

$$Z_h^{-1} = 1 + 4\frac{m_h^2}{v^2}a_{\Box\Box} \tag{3.45}$$

in terms of the operator coefficient $a_{\Box\Box}$ defined in table 1 [101]. We obtain that

$$\kappa_V^{\text{eff}} = \kappa_V + \frac{m_h^2}{v^2}\left(2a_{HWW} + a_{d2} + 2a_{\Box\mathcal{V}\mathcal{V}} - a_{H\mathcal{V}\mathcal{V}} - 2\kappa_V a_{\Box\Box}\right) - \frac{m_W^2}{v^2}4a_{HWW} \tag{3.46}$$

JHEP11(2023)158

$\mathcal{O}_{HWW}$	$-2a_{HWW}\, g_W^2 \frac{h}{v}\mathrm{Tr}\left[W_{\mu\nu}W^{\mu\nu}\right]$	$\mathcal{O}_{H\mathcal{V}\mathcal{V}}$	$-a_{H\mathcal{V}\mathcal{V}}\frac{m_h^2}{2}\frac{h}{v}\mathrm{Tr}\left[\mathcal{V}_\mu\mathcal{V}^\mu\right]$
$\mathcal{O}_{\Box\mathcal{V}\mathcal{V}}$	$a_{\Box\mathcal{V}\mathcal{V}}\frac{\Box h}{v}\mathrm{Tr}\left[\mathcal{V}_\mu\mathcal{V}^\mu\right]$	$\mathcal{O}_{H\Box\Box}$	$a_{H\Box\Box}\frac{h}{v}\frac{\Box h\Box h}{v^2}$
$\mathcal{O}_{d2}$	$ia_{d2}\, g_W \frac{\partial^\nu h}{v}\mathrm{Tr}\left[W_{\mu\nu}\mathcal{V}^\mu\right]$	$\mathcal{O}_{dd\Box}$	$a_{dd\Box}\frac{\partial^\mu h\partial_\mu h}{v^3}$
$\mathcal{O}_{\Box\Box}$	$a_{\Box\Box}\frac{\Box h\Box h}{v^2}$	$\mathcal{O}_{Hdd}$	$a_{Hdd}\frac{m_h^2}{v^2}\frac{h}{v}\partial^\mu h\partial_\mu h$

Table 1. HEFT operators $\mathcal{O}_i$ relevant for the RGE analysis, a_i are the corresponding HEFT coefficients. $\mathcal{V}_\mu = (D_\mu U)U^\dagger$ and $D_\mu\mathcal{V}^\mu = \partial_\mu\mathcal{V}^\mu + i[g_W W_\mu, \mathcal{V}^\mu]$. W, B are the standard gauge field and field strengths. The non-linear sigma model parametrising the Goldstone fields is $\mathrm{U}(\pi^a) = \exp(i\pi^a\tau^a/v)$.

Similarly, from the value of

$$Z_h^{\frac{3}{2}}\hat{\Gamma}_{HHH} \tag{3.47}$$

with all legs on shell we define an effective coupling

$$\kappa_\lambda^{\text{eff}} = \kappa_\lambda + \frac{m_h^2}{v^2}\left(-2a_{H\Box\Box} + a_{dd\Box} - a_{Hdd} - 6\kappa_\lambda a_{\Box\Box}\right) . \tag{3.48}$$

These effective couplings serve the purpose of effectively field-redefining the redundant higher derivative operators generated by the running back into κ_V and κ_λ respectively. We do not define an analogous on-shell κ_{2V}^{eff}, as this would be a complicated function of components of the $hhWW$ effective vertex and components of diagrams containing, e.g., hWW and hhh vertices.

Using the results of [101, 102] (see also [15, 103–107]), the couplings run according to

$$\begin{aligned}
16\pi^2\frac{\mathrm{d}}{\mathrm{d}\log\mu^2}\kappa_V^{\text{eff}} &= \frac{m_h^2}{v^2}\left(\frac{3}{2}(\kappa_{2V}-\kappa_V^2)(\kappa_\lambda-\kappa_V)-\kappa_V(1-\kappa_V^2)\right)\\
&\quad+\frac{m_W^2}{2v^2}\left(3\kappa_V(1-\kappa_V^2)+\frac{20}{3}\kappa_V(\kappa_{2V}-\kappa_V^2)\right)\\
&\quad+\frac{m_Z^2}{2v^2}3\kappa_V(1-\kappa_V^2)\,,\\
16\pi^2\frac{\mathrm{d}}{\mathrm{d}\log\mu^2}\left[\kappa_{2V}-(\kappa_V^{\text{eff}})^2\right] &= \frac{m_h^2}{2v^2}\Big(2(\kappa_{2V}-\kappa_V^2)^2+4\kappa_V^2(1-\kappa_V^2)\\
&\qquad-(\kappa_{2V}-\kappa_V^2)(4\kappa_{2V}-16\kappa_V^2+18\kappa_\lambda\kappa_V-3\kappa_4)\Big)\\
&\quad+\frac{m_W^2}{v^2}\left(3(\kappa_{2V}-\kappa_V^2)^2+\left(3-\frac{20}{3}\kappa_V^2\right)(\kappa_{2V}-\kappa_V^2)\right)\\
&\quad+\frac{m_Z^2}{2v^2}3(\kappa_{2V}-\kappa_V^2)(1-\kappa_V^2)\,,\\
16\pi^2\frac{\mathrm{d}}{\mathrm{d}\log\mu^2}\kappa_\lambda^{\text{eff}} &= \frac{m_h^2}{2v^2}\left(9(\kappa_\lambda-\kappa_V)\kappa_\lambda^2+(\kappa_\lambda+3\kappa_V)(\kappa_{2V}-\kappa_V^2)+6\kappa_\lambda\kappa_4-6\kappa_V^3\right)\\
&\quad+\frac{3(m_W^2+m_Z^2)}{2v^2}3\kappa_\lambda(1-\kappa_V^2)\,.
\end{aligned} \tag{3.49}$$

JHEP11(2023)158

κ_4 is the multiplicative modifier of the h^4 vertex, and is set to one in the following. We have chosen to present the running of κ_{2V} in terms of that of the combination $\kappa_{2V} - (\kappa_V^{\text{eff}})^2$, which controls the energy growth of the $WW \to hh$ process.

The Standard Model is a fixed point of the running, as the RHSs of eq. (3.49) vanish when $\kappa_V = \kappa_{2V} = \kappa_\lambda = 1$.[7] Linearising the RGEs about this point by defining

$$\begin{aligned} \delta\kappa_V &= \kappa_V^{\text{eff}} - 1\,, \\ \delta K_{2V} &= \kappa_{2V} - (\kappa_V^{\text{eff}})^2\,, \\ \delta\kappa_\lambda &= \kappa_\lambda^{\text{eff}} - 1\,, \end{aligned} \tag{3.50}$$

we find

$$\begin{aligned} 16\pi^2 \frac{\mathrm{d}}{\mathrm{d}\log\mu^2}\delta\kappa_V &= \delta\kappa_V\left(2\frac{m_h^2}{v^2} - \frac{3(m_W^2+m_Z^2)}{2v^2}\right) + \delta K_{2V}\left(\frac{3m_W^2}{v^2}\right) \\ 16\pi^2 \frac{\mathrm{d}}{\mathrm{d}\log\mu^2}\delta K_{2V} &= \delta\kappa_V\left(-4\frac{m_h^2}{v^2}\right) + \delta K_{2V}\left(-\frac{3m_h^2}{2v^2} - \frac{40m_W^2}{3v^2}\right) \\ 16\pi^2 \frac{\mathrm{d}}{\mathrm{d}\log\mu^2}\delta\kappa_\lambda &= \delta\kappa_V\left(-\frac{27m_h^2}{2v^2} - \frac{9(m_W^2+m_Z^2)}{2v^2}\right) + \delta K_{2V}\left(\frac{2m_h^2}{v^2}\right) + \delta\kappa_\lambda\left(\frac{15m_h^2}{2v^2}\right) \end{aligned} \tag{3.51}$$

up to $\mathrm{O}((\delta\kappa)^2)$ corrections. Note that, to expand the r.h.s. of eq. (3.49), we have assumed we are running from a point where all higher order a coefficients are zero.

We note from eq. (3.51) that $\delta\kappa_\lambda$, which is experimentally the least constrained of the three parameters, self-renormalises significantly stronger than the other two. Also, the negative coefficient for the self-renormalisation of δK_{2V} means that a positive δK_{2V}, as is the case for all renormalisable models, grows in the IR, away from the $\delta K_{2V} = 0$ alignment limit.

4 Conclusions

Analyses employing Feynman diagrams as templates are established approaches in the experimental community [2, 47] in situations where data is expected to be limited, even at the high-luminosity phase of the LHC or stretches of future collider runs. What can be learned from them? To answer this question and provide an ab initio motivation for these analyses, we have performed such a templated analysis of future sensitivity in the WBF di-Higgs channel to the coupling modifiers $\kappa_{2V}, \kappa_V, \kappa_\lambda$, and we have scanned a range of BSM models to understand their pattern of effects in the same three coupling modifiers.

Figure 7 shows projected future constraints on the κ_V-κ_{2V} plane from the WBF di-Higgs process. This translates into approximate 2σ bounds on deviations in the single parameter κ_{2V} of order 30% for HL-LHC, and order 5% for future colliders. These are to be contrasted with bounds on κ_V from single Higgs measurements that are approximately an order of magnitude smaller.

On the theoretical side, deviations in κ_{2V} and κ_V are highly correlated in all models of heavy, decoupling new physics. This can be understood through their SMEFT parametrisation, where, due to the doublet nature of the Higgs field, $\kappa_{2V} = 2\kappa_V^2 - 1$ at dimension 6. In

[7] Without defining $\kappa_\lambda^{\text{eff}}$ to take account of the effect of the higher derivative operators, κ_λ would appear to run even at the Standard Model point.

JHEP11(2023)158

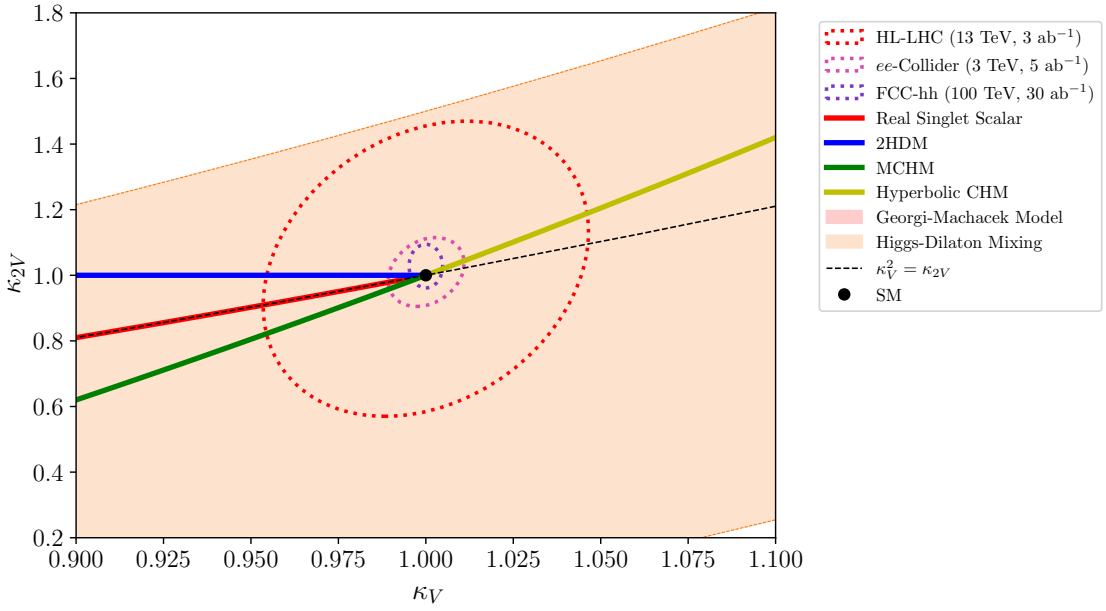

Figure 7. κ_V-κ_{2V} correlation for different 95% CL collider sensitivity extrapolations, assuming $\kappa_\lambda = 1$. We overlay the BSM model discussion of section 3 to highlight regions for which κ_{2V} can provide information beyond κ_V. In particular, the fourth quadrant (where $\kappa_{2V} < 1 < \kappa_V$) is populated by scenarios of large dilaton-Higgs mixing (we scan $-1 \leq \kappa_{2V} \leq 2, |s_\theta| \leq 1$ with a physical solution of $\zeta > 0$; again we assume $M_{hh} = 300$ GeV as before). Note that the dilaton includes effects beyond the deformation truncated in eq. (3.38). Hence, the covered area is comparably larger. The black dashed line represents $\kappa_V^2 = \kappa_{2V}$ and all BSM renormalisable models lie in the region above this line, i.e., $\kappa_V^2 \leq \kappa_{2V}$.

the broader HEFT parametrisation, κ_{2V} and κ_V are independent free parameters due to the custodial iso-singlet parameterisation of the Higgs boson. Any models of non-decoupling new physics where the deviation in κ_{2V} is an order of magnitude larger than that in κ_V would highly motivate WBF di-Higgs production as an indirect probe of new physics.

To this end, we surveyed many BSM models in section 3, and summarise their patterns of effects in κ_{2V} and κ_V in table 2. In sum, to achieve an enhancement in κ_{2V} within an extended scalar sector requires tree-level mixing with triplets or higher electroweak representations. This cannot be done at loop level, where extra scalars give a characteristic $\kappa_{2V} = \kappa_V^2$ pattern from wavefunction renormalisation of the Higgs. We note in passing, however, that we have identified a large class of scalar extensions of the SM for which a Feynman-templated analysis extends to one-loop BSM precision in the weak sector.

We find that all renormalisable extended scalar sectors satisfy $\kappa_{2V} - \kappa_V^2 \geq 0$, with this quantity growing in the IR due to running effects. As $\kappa_{2V} - \kappa_V^2$ also controls the energy growth of longitudinal W-Higgs scattering, it is possible that a sum rule type argument could yield further insight into this sign. $\kappa_{2V} - \kappa_V^2 < 0$ is achievable, however, in non-renormalisable models of the scalar sector. The archetype of such a model — the minimal composite Higgs model — follows the SMEFT pattern, as it smoothly decouples in the $f \to \infty$ limit. However, it is possible to obtain a large (and negative) deviation in κ_{2V} in composite Higgs models which contain a TeV scale dilaton.

JHEP11(2023)158

Model	κ_V	κ_{2V}	Ref.
Singlet	$\cos\alpha$	$\cos^2\alpha$	Section A.1
2HDM	$\sin(\alpha-\beta)$	1	Section A.2
Georgi-Machacek	$\cos\alpha\cos\beta+2\sqrt{\frac{2}{3}}\sin\alpha\sin\beta$	$\cos^2\alpha+\frac{8}{3}\sin^2\alpha$	Section A.3
Tree-level scalar	$\frac{C_{ij}v_i\hat{n}_j}{(C_{ij}v_iv_j)^{\frac{1}{2}}}$	$C_{ij}\hat{n}_i\hat{n}_j$	Section 3.1
Loop-level scalar (large λ)	$1-D\,\frac{\lambda^2v^2}{96\pi^2m_\varphi^2}$	$1-D\,\frac{\lambda^2v^2}{48\pi^2m_\varphi^2}$	Section 3.2
SMEFT	free	$\simeq 2\kappa_V^2-1$	e.g. [10, 108]
MCHM	$\sqrt{1-\xi}$	$1-2\xi$	Section 3.3
MCHM + Dilaton	$c_\phi\sqrt{1-\xi}-s_\phi\sqrt{\zeta}$	$(1-2\xi)c_\phi^2+\zeta s_\phi^2-2\sqrt{\zeta(1-\xi)}s_{2\phi}$	Section 3.3
HEFT	free	free	e.g. [102]

Table 2. A collection of κ_V, κ_{2V} values of the simplified models described in section 3 and appendix A.

Our investigation therefore shows that the Feynman diagram-based explorations of the WBF channel add important value to the phenomenology programme, at the LHC and beyond. κ_{2V} can significantly depart from the SM correlation with κ_V, and the loose constraints on κ_{2V} probe parameter regions of BSM scenario that are not accessible by a precision study of κ_V alone. This is assisted by considerable stability of the WBF cross sections from the point of view of QCD. However, measurable deviations in κ_{2V} come at the price of significant tree-level mixing at the TeV scale in either perturbative (extended scalar sectors containing higher electroweak irreps) or non-perturbative (composite Higgs with dilaton) scenarios. The size of tree-level mixing highlights the relevance of direct searches. To compare the power of direct searches, let us briefly consider the prospects at the LHC for the Georgi-Machacek and composite Higgs with dilaton models.

For the Georgi-Machacek model, tell-tale and experimentally clean signatures arise from the doubly charged, gauge-philic Higgs boson, whose interactions are sensitive to the triplets' contribution to the electroweak vacuum. Recent constraints [109] limit $|\sin\beta| \lesssim 0.2$ for masses below 1 TeV. A luminosity-based extrapolation should further decrease this by a factor of two for HL-LHC. Using the expressions in table 2 with $|\sin\beta| \lesssim 0.2(0.1)$ and $\kappa_V = 1$ gives a possible range of $1 \leq \kappa_{2V} \lesssim 1.5(1.15)$ from current (future) LHC resonance searches, which is comparable to the κ_{2V} constraints from di-Higgs measurements.

For the composite Higgs models, including those which mix with a dilaton, one expects other composite resonances to appear at a scale below $4\pi f \gtrsim 5\,\text{TeV}$, assuming $f \gtrsim 500\,\text{GeV}$. Arguably, the most model independent predictions of the composite Higgs do not yet meet this threshold: the pair production of top partners is currently bounded up to masses of around 1.5 TeV [110], and the electroweak production and decay of a heavy vector triplet — analogous to $\pi\pi \to \rho \to \pi\pi$ in QCD — is currently bounded up to masses of around 4 TeV [111]. This latter bound is limited by the collision energy of the LHC, and is unlikely to improve significantly with increased luminosity. Therefore, using the expressions in

JHEP11(2023)158

table 2 with $f, \langle\chi\rangle \gtrsim 500\,\text{GeV}$ and $\kappa_V = 1$ gives a possible range of $0.0 \lesssim \kappa_{2V} \lesssim 1.3$. We note that, if the dilaton has (model dependently) a coupling to gluons, a direct search for the dilaton in $gg \to \chi \to WW/ZZ$ could rule out a significant amount of this parameter space [96].

Finally, although κ_λ plays a subdominant phenomenological role in WBF hh production in a hadron collider, in many of the scenarios that we have considered in this work, κ_λ more susceptible to deviations from the SM compared to κ_{2V}, κ_V. Examples include tree-level extended scalar sectors in the alignment with decoupling limit, loop-level scalars with sizeable cross-quartic interactions with the Higgs doublet, and composite Higgs models containing explicit symmetry breaking terms in higher spurionic irreps. As κ_λ can be dominantly extracted from $gg \to hh$ analyses, correlations observed in the WBF mode will add further exclusion potential.

Acknowledgments

We thank Aidan Robson and Panagiotis Stylianou for helpful conversations. C.E. is supported by the STFC under grants ST/T000945/1, ST/X000605/1, and the Leverhulme Trust under grant RPG-2021-031. C.E. and D.S. acknowledge support from the Institute for Particle Physics Phenomenology Associateship Scheme. W.N. is funded by a University of Glasgow College of Science and Engineering Scholarship.

A κ_V and κ_{2V} in specific scalar models

Here we give the κ_V and κ_{2V} values at tree level in specific extended scalar sectors, using the master formulae eqs. (3.6) and (3.9).

A.1 Higgs + singlet

In unitary gauge, there is one neutral component of the Higgs doublet and one from the singlet, with C matrix

$$C_{ij} = \begin{pmatrix} 1 & 0 \\ 0 & 0 \end{pmatrix} . \tag{A.1}$$

Writing $v_i = (v_1, v_2)^T$ and $\hat{n}_i = (\cos\alpha, \sin\alpha)^T$, we have

$$\kappa_V = \cos\alpha\,, \tag{A.2}$$

$$\kappa_{2V} = \cos^2\alpha\,, \tag{A.3}$$

as expected.

A.2 2HDM

In unitary gauge there are two scalar neutral components, which both generically contain vevs and mix among each other, and a pseudoscalar neutral component which, when custodial symmetry is imposed, obtains no vev and does not mix with the other neutral

JHEP11(2023)158

components [70] (see the recent [112] for the 2HDMs relation to HEFT). The C matrix is the identity matrix,

$$C_{ij} = \begin{pmatrix} 1 & 0 & 0 \\ 0 & 1 & 0 \\ 0 & 0 & 1 \end{pmatrix} . \tag{A.4}$$

Writing

$$\hat{n}_i = (\sin\alpha, \cos\alpha, 0)^T \tag{A.5}$$

$$v_i = v\,(\cos\beta, \sin\beta, 0)^T \tag{A.6}$$

where the third entry is associated with the pseudoscalar component, we obtain

$$\kappa_V = \sin(\alpha - \beta)\,, \tag{A.7}$$

$$\kappa_{2V} = 1\,. \tag{A.8}$$

A.3 Georgi-Machacek

Ordering the neutral components respectively as that of the Higgs doublet, the two components of the complex $Y = 1$ triplet and the one component of the real $Y = 0$ triplet, the C matrix is

$$C_{ij} = \begin{pmatrix} 1 & 0 & 0 & 0 \\ 0 & 2 & 0 & 0 \\ 0 & 0 & 2 & 0 \\ 0 & 0 & 0 & 4 \end{pmatrix} \tag{A.9}$$

Custodial symmetry implies that $v_2 = v_3 = v_4$ among the triplet components, and also that the mass matrix is invariant under permutations among the 2, 3 and 4 indices, meaning $n_2 = n_3 = n_4$ in the light Higgs eigenvector [113]. Thus we can write

$$\hat{n}_i = \left(\cos\alpha, \frac{1}{\sqrt{3}}\sin\alpha, \frac{1}{\sqrt{3}}\sin\alpha, \frac{1}{\sqrt{3}}\sin\alpha\right)^T \tag{A.10}$$

$$v_i = v\left(\cos\beta, \frac{1}{2\sqrt{2}}\sin\beta, \frac{1}{2\sqrt{2}}\sin\beta, \frac{1}{2\sqrt{2}}\sin\beta\right)^T \tag{A.11}$$

which implies that

$$\kappa_V = \cos\beta\cos\alpha + 2\sqrt{\frac{2}{3}}\sin\beta\sin\alpha\,, \tag{A.12}$$

$$\kappa_{2V} = \cos^2\alpha + \frac{8}{3}\sin^2\alpha\,. \tag{A.13}$$

We have also reproduced this result using the mass matrices of [113], see also [69].

JHEP11(2023)158

References

[1] LHC Higgs Cross Section Working Group collaboration, *Handbook of LHC Higgs Cross Sections: 1. Inclusive Observables*, arXiv:1101.0593 [DOI:10.5170/CERN-2011-002] [INSPIRE].

[2] ATLAS collaboration, *Search for nonresonant pair production of Higgs bosons in the $b\bar{b}b\bar{b}$ final state in pp collisions at $\sqrt{s} = 13$ TeV with the ATLAS detector*, *Phys. Rev. D* **108** (2023) 052003 [arXiv:2301.03212] [INSPIRE].

[3] ATLAS collaboration, *Searches for Higgs boson pair production in the $hh \to bb\tau\tau, \gamma\gamma WW^*, \gamma\gamma bb, bbbb$ channels with the ATLAS detector*, *Phys. Rev. D* **92** (2015) 092004 [arXiv:1509.04670] [INSPIRE].

[4] CMS collaboration, *Search for Higgs boson pair production in events with two bottom quarks and two tau leptons in proton-proton collisions at $\sqrt{s} = 13$ TeV*, *Phys. Lett. B* **778** (2018) 101 [arXiv:1707.02909] [INSPIRE].

[5] CMS collaboration, *Search for Higgs boson pair production in the $bb\tau\tau$ final state in proton-proton collisions at $\sqrt{s} = 8$ TeV*, *Phys. Rev. D* **96** (2017) 072004 [arXiv:1707.00350] [INSPIRE].

[6] CMS collaboration, *Search for nonresonant Higgs boson pair production in final states with two bottom quarks and two photons in proton-proton collisions at $\sqrt{s} = 13$ TeV*, *JHEP* **03** (2021) 257 [arXiv:2011.12373] [INSPIRE].

[7] ATLAS collaboration, *Search for Higgs boson pair production in the two bottom quarks plus two photons final state in pp collisions at $\sqrt{s} = 13$ TeV with the ATLAS detector*, *Phys. Rev. D* **106** (2022) 052001 [arXiv:2112.11876] [INSPIRE].

[8] CMS collaboration, *Search for nonresonant Higgs boson pair production in final state with two bottom quarks and two tau leptons in proton-proton collisions at $\sqrt{s} = 13$ TeV*, *Phys. Lett. B* **842** (2023) 137531 [arXiv:2206.09401] [INSPIRE].

[9] ATLAS collaboration, *Search for resonant and non-resonant Higgs boson pair production in the $b\bar{b}\tau^+\tau^-$ decay channel using 13 TeV pp collision data from the ATLAS detector*, *JHEP* **07** (2023) 040 [arXiv:2209.10910] [INSPIRE].

[10] B. Grzadkowski, M. Iskrzynski, M. Misiak and J. Rosiek, *Dimension-Six Terms in the Standard Model Lagrangian*, *JHEP* **10** (2010) 085 [arXiv:1008.4884] [INSPIRE].

[11] M. McCullough, *An Indirect Model-Dependent Probe of the Higgs Self-Coupling*, *Phys. Rev. D* **90** (2014) 015001 [*Erratum ibid.* **92** (2015) 039903] [arXiv:1312.3322] [INSPIRE].

[12] G. Degrassi, P.P. Giardino, F. Maltoni and D. Pagani, *Probing the Higgs self coupling via single Higgs production at the LHC*, *JHEP* **12** (2016) 080 [arXiv:1607.04251] [INSPIRE].

[13] M. Gorbahn and U. Haisch, *Indirect probes of the trilinear Higgs coupling: $gg \to h$ and $h \to \gamma\gamma$*, *JHEP* **10** (2016) 094 [arXiv:1607.03773] [INSPIRE].

[14] G.D. Kribs et al., *Electroweak oblique parameters as a probe of the trilinear Higgs boson self-interaction*, *Phys. Rev. D* **95** (2017) 093004 [arXiv:1702.07678] [INSPIRE].

[15] Anisha et al., *Quartic Gauge-Higgs couplings: constraints and future directions*, *JHEP* **10** (2022) 172 [arXiv:2208.09334] [INSPIRE].

[16] K. Agashe, R. Contino and A. Pomarol, *The Minimal composite Higgs model*, *Nucl. Phys. B* **719** (2005) 165 [hep-ph/0412089] [INSPIRE].

JHEP11(2023)158

[17] R. Contino, L. Da Rold and A. Pomarol, *Light custodians in natural composite Higgs models*, *Phys. Rev. D* **75** (2007) 055014 [hep-ph/0612048] [INSPIRE].

[18] S.R. Coleman, J. Wess and B. Zumino, *Structure of phenomenological Lagrangians. 1*, *Phys. Rev.* **177** (1969) 2239 [INSPIRE].

[19] C.G. Callan Jr., S.R. Coleman, J. Wess and B. Zumino, *Structure of phenomenological Lagrangians. 2*, *Phys. Rev.* **177** (1969) 2247 [INSPIRE].

[20] T. Binoth and J.J. van der Bij, *Influence of strongly coupled, hidden scalars on Higgs signals*, *Z. Phys. C* **75** (1997) 17 [hep-ph/9608245] [INSPIRE].

[21] B. Patt and F. Wilczek, *Higgs-field portal into hidden sectors*, hep-ph/0605188 [INSPIRE].

[22] R.M. Schabinger and J.D. Wells, *A Minimal spontaneously broken hidden sector and its impact on Higgs boson physics at the large hadron collider*, *Phys. Rev. D* **72** (2005) 093007 [hep-ph/0509209] [INSPIRE].

[23] C. Englert, T. Plehn, D. Zerwas and P.M. Zerwas, *Exploring the Higgs portal*, *Phys. Lett. B* **703** (2011) 298 [arXiv:1106.3097] [INSPIRE].

[24] R. Alonso, E.E. Jenkins and A.V. Manohar, *A Geometric Formulation of Higgs Effective Field Theory: Measuring the Curvature of Scalar Field Space*, *Phys. Lett. B* **754** (2016) 335 [arXiv:1511.00724] [INSPIRE].

[25] S. Dawson, *The Effective W Approximation*, *Nucl. Phys. B* **249** (1985) 42 [INSPIRE].

[26] R. Contino et al., *Strong Double Higgs Production at the LHC*, *JHEP* **05** (2010) 089 [arXiv:1002.1011] [INSPIRE].

[27] T. Hahn and M. Perez-Victoria, *Automatized one loop calculations in four-dimensions and D-dimensions*, *Comput. Phys. Commun.* **118** (1999) 153 [hep-ph/9807565] [INSPIRE].

[28] T. Hahn, *Automatic loop calculations with FeynArts, FormCalc, and LoopTools*, *Nucl. Phys. B Proc. Suppl.* **89** (2000) 231 [hep-ph/0005029] [INSPIRE].

[29] T. Hahn, *Generating Feynman diagrams and amplitudes with FeynArts 3*, *Comput. Phys. Commun.* **140** (2001) 418 [hep-ph/0012260] [INSPIRE].

[30] L. Di Luzio, R. Gröber and M. Spannowsky, *Maxi-sizing the trilinear Higgs self-coupling: how large could it be?*, *Eur. Phys. J. C* **77** (2017) 788 [arXiv:1704.02311] [INSPIRE].

[31] F. Arco, S. Heinemeyer and M.J. Herrero, *Exploring sizable triple Higgs couplings in the 2HDM*, *Eur. Phys. J. C* **80** (2020) 884 [arXiv:2005.10576] [INSPIRE].

[32] F. Arco, S. Heinemeyer, M. Mühlleitner and K. Radchenko, *Sensitivity to triple Higgs couplings via di-Higgs production in the 2HDM at the (HL-)LHC*, *Eur. Phys. J. C* **83** (2023) 1019 [arXiv:2212.11242] [INSPIRE].

[33] R.N. Cahn and S. Dawson, *Production of Very Massive Higgs Bosons*, *Phys. Lett. B* **136** (1984) 196 [*Erratum ibid.* **138** (1984) 464] [INSPIRE].

[34] D.L. Rainwater, D. Zeppenfeld and K. Hagiwara, *Searching for $H \to \tau^+\tau^-$ in weak boson fusion at the CERN LHC*, *Phys. Rev. D* **59** (1998) 014037 [hep-ph/9808468] [INSPIRE].

[35] D. Zeppenfeld, R. Kinnunen, A. Nikitenko and E. Richter-Was, *Measuring Higgs boson couplings at the CERN LHC*, *Phys. Rev. D* **62** (2000) 013009 [hep-ph/0002036] [INSPIRE].

[36] T. Figy, C. Oleari and D. Zeppenfeld, *Next-to-leading order jet distributions for Higgs boson production via weak boson fusion*, *Phys. Rev. D* **68** (2003) 073005 [hep-ph/0306109] [INSPIRE].

JHEP11(2023)158

[37] T. Figy, *Next-to-leading order QCD corrections to light Higgs Pair production via vector boson fusion*, *Mod. Phys. Lett. A* **23** (2008) 1961 [arXiv:0806.2200] [INSPIRE].

[38] F.A. Dreyer and A. Karlberg, *Vector-Boson Fusion Higgs Pair Production at N^3LO*, *Phys. Rev. D* **98** (2018) 114016 [arXiv:1811.07906] [INSPIRE].

[39] K. Arnold et al., *VBFNLO: A Parton level Monte Carlo for processes with electroweak bosons*, *Comput. Phys. Commun.* **180** (2009) 1661 [arXiv:0811.4559] [INSPIRE].

[40] J. Baglio et al., *The measurement of the Higgs self-coupling at the LHC: theoretical status*, *JHEP* **04** (2013) 151 [arXiv:1212.5581] [INSPIRE].

[41] J. Alwall et al., *The automated computation of tree-level and next-to-leading order differential cross sections, and their matching to parton shower simulations*, *JHEP* **07** (2014) 079 [arXiv:1405.0301] [INSPIRE].

[42] R. Frederix et al., *Higgs pair production at the LHC with NLO and parton-shower effects*, *Phys. Lett. B* **732** (2014) 142 [arXiv:1401.7340] [INSPIRE].

[43] FCC collaboration, *FCC-hh: The Hadron Collider: Future Circular Collider Conceptual Design Report Volume 3*, *Eur. Phys. J. ST* **228** (2019) 755 [INSPIRE].

[44] ATLAS collaboration, *Search for pair production of Higgs bosons in the $b\bar{b}b\bar{b}$ final state using proton-proton collisions at $\sqrt{s} = 13$ TeV with the ATLAS detector*, *JHEP* **01** (2019) 030 [arXiv:1804.06174] [INSPIRE].

[45] ATLAS collaboration, *Search for the $HH \to b\bar{b}b\bar{b}$ process via vector-boson fusion production using proton-proton collisions at $\sqrt{s} = 13$ TeV with the ATLAS detector*, *JHEP* **07** (2020) 108 [*Erratum ibid.* **01** (2021) 145] [arXiv:2001.05178] [INSPIRE].

[46] CMS collaboration, *Search for Higgs Boson Pair Production in the Four b Quark Final State in Proton-Proton Collisions at $\sqrt{s} = 13$ TeV*, *Phys. Rev. Lett.* **129** (2022) 081802 [arXiv:2202.09617] [INSPIRE].

[47] CMS collaboration, *Search for Nonresonant Pair Production of Highly Energetic Higgs Bosons Decaying to Bottom Quarks*, *Phys. Rev. Lett.* **131** (2023) 041803 [arXiv:2205.06667] [INSPIRE].

[48] C. Bierlich et al., *A comprehensive guide to the physics and usage of PYTHIA 8.3*, arXiv:2203.11601 [DOI:10.21468/SciPostPhysCodeb.8] [INSPIRE].

[49] E. Conte, B. Fuks and G. Serret, *MadAnalysis 5, A User-Friendly Framework for Collider Phenomenology*, *Comput. Phys. Commun.* **184** (2013) 222 [arXiv:1206.1599] [INSPIRE].

[50] M. Cacciari, G.P. Salam and G. Soyez, *FastJet User Manual*, *Eur. Phys. J. C* **72** (2012) 1896 [arXiv:1111.6097] [INSPIRE].

[51] M. Cacciari and G.P. Salam, *Dispelling the N^3 myth for the k_t jet-finder*, *Phys. Lett. B* **641** (2006) 57 [hep-ph/0512210] [INSPIRE].

[52] M.J. Dolan, C. Englert, N. Greiner and M. Spannowsky, *Further on up the road: hhjj production at the LHC*, *Phys. Rev. Lett.* **112** (2014) 101802 [arXiv:1310.1084] [INSPIRE].

[53] M.J. Dolan et al., *hhjj production at the LHC*, *Eur. Phys. J. C* **75** (2015) 387 [arXiv:1506.08008] [INSPIRE].

[54] F. Bishara, R. Contino and J. Rojo, *Higgs pair production in vector-boson fusion at the LHC and beyond*, *Eur. Phys. J. C* **77** (2017) 481 [arXiv:1611.03860] [INSPIRE].

JHEP11(2023)158

[55] ATLAS collaboration, *A detailed map of Higgs boson interactions by the ATLAS experiment ten years after the discovery*, *Nature* **607** (2022) 52 [*Erratum ibid.* **612** (2022) E24] [arXiv:2207.00092] [INSPIRE].

[56] Z. Chacko, C. Kilic, S. Najjari and C.B. Verhaaren, *Testing the Scalar Sector of the Twin Higgs Model at Colliders*, *Phys. Rev. D* **97** (2018) 055031 [arXiv:1711.05300] [INSPIRE].

[57] S. Di Vita et al., *A global view on the Higgs self-coupling at lepton colliders*, *JHEP* **02** (2018) 178 [arXiv:1711.03978] [INSPIRE].

[58] B. Li, Z.-L. Han and Y. Liao, *Higgs production at future e^+e^- colliders in the Georgi-Machacek model*, *JHEP* **02** (2018) 007 [arXiv:1710.00184] [INSPIRE].

[59] H. Abramowicz et al., *Higgs physics at the CLIC electron-positron linear collider*, *Eur. Phys. J. C* **77** (2017) 475 [arXiv:1608.07538] [INSPIRE].

[60] D. Domenech, M.J. Herrero, R.A. Morales and M. Ramos, *Double Higgs boson production at TeV e^+e^- colliders with effective field theories: Sensitivity to BSM Higgs couplings*, *Phys. Rev. D* **106** (2022) 115027 [arXiv:2208.05452] [INSPIRE].

[61] M. Gonzalez-Lopez, M.J. Herrero and P. Martinez-Suarez, *Testing anomalous $H-W$ couplings and Higgs self-couplings via double and triple Higgs production at e^+e^- colliders*, *Eur. Phys. J. C* **81** (2021) 260 [arXiv:2011.13915] [INSPIRE].

[62] CLICDP collaboration, *Double Higgs boson production and Higgs self-coupling extraction at CLIC*, *Eur. Phys. J. C* **80** (2020) 1010 [arXiv:1901.05897] [INSPIRE].

[63] J. de Blas et al., *Higgs Boson Studies at Future Particle Colliders*, *JHEP* **01** (2020) 139 [arXiv:1905.03764] [INSPIRE].

[64] M. Cepeda et al., *Report from Working Group 2: Higgs Physics at the HL-LHC and HE-LHC*, *CERN Yellow Rep. Monogr.* **7** (2019) 221 [arXiv:1902.00134] [INSPIRE].

[65] R. Contino et al., *Physics at a 100 TeV pp collider: Higgs and EW symmetry breaking studies*, arXiv:1606.09408 [DOI:10.23731/CYRM-2017-003.255] [INSPIRE].

[66] ILC collaboration, *The International Linear Collider. A Global Project*, arXiv:1901.09829 [INSPIRE].

[67] U. Baur, T. Plehn and D.L. Rainwater, *Measuring the Higgs Boson Self Coupling at the LHC and Finite Top Mass Matrix Elements*, *Phys. Rev. Lett.* **89** (2002) 151801 [hep-ph/0206024] [INSPIRE].

[68] M.J. Dolan, C. Englert and M. Spannowsky, *Higgs self-coupling measurements at the LHC*, *JHEP* **10** (2012) 112 [arXiv:1206.5001] [INSPIRE].

[69] R. Alonso and M. West, *Roads to the Standard Model*, *Phys. Rev. D* **105** (2022) 096028 [arXiv:2109.13290] [INSPIRE].

[70] J.F. Gunion, R. Vega and J. Wudka, *Higgs triplets in the standard model*, *Phys. Rev. D* **42** (1990) 1673 [INSPIRE].

[71] C. Englert, E. Re and M. Spannowsky, *Pinning down Higgs triplets at the LHC*, *Phys. Rev. D* **88** (2013) 035024 [arXiv:1306.6228] [INSPIRE].

[72] CMS collaboration, *Search for charged Higgs bosons produced in vector boson fusion processes and decaying into vector boson pairs in proton-proton collisions at $\sqrt{s} = 13$ TeV*, *Eur. Phys. J. C* **81** (2021) 723 [arXiv:2104.04762] [INSPIRE].

JHEP11(2023)158

[73] A. Ismail, H.E. Logan and Y. Wu, *Updated constraints on the Georgi-Machacek model from LHC Run 2*, arXiv:2003.02272 [INSPIRE].

[74] D. Egana-Ugrinovic and S. Thomas, *Effective Theory of Higgs Sector Vacuum States*, arXiv:1512.00144 [INSPIRE].

[75] I. Banta et al., *Non-decoupling new particles*, *JHEP* **02** (2022) 029 [arXiv:2110.02967] [INSPIRE].

[76] I. Banta, *A strongly first-order electroweak phase transition from Loryons*, *JHEP* **06** (2022) 099 [arXiv:2202.04608] [INSPIRE].

[77] D.A. Ross and J.C. Taylor, *Renormalization of a unified theory of weak and electromagnetic interactions*, *Nucl. Phys. B* **51** (1973) 125 [INSPIRE].

[78] A. Denner, S. Dittmaier and J.-N. Lang, *Renormalization of mixing angles*, *JHEP* **11** (2018) 104 [arXiv:1808.03466] [INSPIRE].

[79] A. Sirlin, *Radiative Corrections in the* $\mathrm{SU}(2)_L \times \mathrm{U}(1)$ *Theory: A Simple Renormalization Framework*, *Phys. Rev. D* **22** (1980) 971 [INSPIRE].

[80] G. Passarino and M.J.G. Veltman, *One Loop Corrections for* e^+e^- *Annihilation Into* $\mu^+\mu^-$ *in the Weinberg Model*, *Nucl. Phys. B* **160** (1979) 151 [INSPIRE].

[81] A. Djouadi, *The Anatomy of electro-weak symmetry breaking. I: The Higgs boson in the standard model*, *Phys. Rept.* **457** (2008) 1 [hep-ph/0503172] [INSPIRE].

[82] D. Carmi et al., *Higgs After the Discovery: A Status Report*, *JHEP* **10** (2012) 196 [arXiv:1207.1718] [INSPIRE].

[83] R. Contino, Y. Nomura and A. Pomarol, *Higgs as a holographic pseudoGoldstone boson*, *Nucl. Phys. B* **671** (2003) 148 [hep-ph/0306259] [INSPIRE].

[84] R. Alonso, E.E. Jenkins and A.V. Manohar, *Sigma Models with Negative Curvature*, *Phys. Lett. B* **756** (2016) 358 [arXiv:1602.00706] [INSPIRE].

[85] R. Alonso, E.E. Jenkins and A.V. Manohar, *Geometry of the Scalar Sector*, *JHEP* **08** (2016) 101 [arXiv:1605.03602] [INSPIRE].

[86] G. Ferretti, *UV Completions of Partial Compositeness: The Case for a* SU(4) *Gauge Group*, *JHEP* **06** (2014) 142 [arXiv:1404.7137] [INSPIRE].

[87] R. Contino, *The Higgs as a Composite Nambu-Goldstone Boson*, in the proceedings of the *Theoretical Advanced Study Institute in Elementary Particle Physics: Physics of the Large and the Small*, Boulder, Colorado, U.S.A., 1–26 June 2009 (2011), p. 235–306 [DOI:10.1142/9789814327183_0005] [arXiv:1005.4269] [INSPIRE].

[88] M. Golterman and Y. Shamir, *Top quark induced effective potential in a composite Higgs model*, *Phys. Rev. D* **91** (2015) 094506 [arXiv:1502.00390] [INSPIRE].

[89] L. Del Debbio, C. Englert and R. Zwicky, *A UV Complete Compositeness Scenario: LHC Constraints Meet The Lattice*, *JHEP* **08** (2017) 142 [arXiv:1703.06064] [INSPIRE].

[90] V. Ayyar et al., *Partial compositeness and baryon matrix elements on the lattice*, *Phys. Rev. D* **99** (2019) 094502 [arXiv:1812.02727] [INSPIRE].

[91] L. Del Debbio, A. Lupo, M. Panero and N. Tantalo, *Multi-representation dynamics of* SU(4) *composite Higgs models: chiral limit and spectral reconstructions*, *Eur. Phys. J. C* **83** (2023) 220 [arXiv:2211.09581] [INSPIRE].

JHEP11(2023)158

[92] R. Gröber and M. Mühlleitner, *Composite Higgs Boson Pair Production at the LHC*, *JHEP* **06** (2011) 020 [arXiv:1012.1562] [INSPIRE].

[93] G. Durieux, M. McCullough and E. Salvioni, *Gegenbauer Goldstones*, *JHEP* **01** (2022) 076 [arXiv:2110.06941] [INSPIRE].

[94] J.A. Wolf, *Spaces of constant curvature*, AMS Chelsea Pub., Providence, RI, U.S.A. (2011).

[95] J.D. Bekenstein, *The Relation between physical and gravitational geometry*, *Phys. Rev. D* **48** (1993) 3641 [gr-qc/9211017] [INSPIRE].

[96] S. Bruggisser, B. von Harling, O. Matsedonskyi and G. Servant, *Dilaton at the LHC: complementary probe of composite Higgs*, *JHEP* **05** (2023) 080 [arXiv:2212.00056] [INSPIRE].

[97] W.D. Goldberger, B. Grinstein and W. Skiba, *Distinguishing the Higgs boson from the dilaton at the Large Hadron Collider*, *Phys. Rev. Lett.* **100** (2008) 111802 [arXiv:0708.1463] [INSPIRE].

[98] R. Rattazzi and A. Zaffaroni, *Comments on the holographic picture of the Randall-Sundrum model*, *JHEP* **04** (2001) 021 [hep-th/0012248] [INSPIRE].

[99] Z. Komargodski and A. Schwimmer, *On Renormalization Group Flows in Four Dimensions*, *JHEP* **12** (2011) 099 [arXiv:1107.3987] [INSPIRE].

[100] M.J. Dolan, C. Englert and M. Spannowsky, *New Physics in LHC Higgs boson pair production*, *Phys. Rev. D* **87** (2013) 055002 [arXiv:1210.8166] [INSPIRE].

[101] M.J. Herrero and R.A. Morales, *One-loop corrections for WW to HH in Higgs EFT with the electroweak chiral Lagrangian*, *Phys. Rev. D* **106** (2022) 073008 [arXiv:2208.05900] [INSPIRE].

[102] M.J. Herrero and R.A. Morales, *One-loop renormalization of vector boson scattering with the electroweak chiral Lagrangian in covariant gauges*, *Phys. Rev. D* **104** (2021) 075013 [arXiv:2107.07890] [INSPIRE].

[103] R.L. Delgado, A. Dobado and F.J. Llanes-Estrada, *One-loop W_LW_L and Z_LZ_L scattering from the electroweak Chiral Lagrangian with a light Higgs-like scalar*, *JHEP* **02** (2014) 121 [arXiv:1311.5993] [INSPIRE].

[104] M.B. Gavela, K. Kanshin, P.A.N. Machado and S. Saa, *On the renormalization of the electroweak chiral Lagrangian with a Higgs*, *JHEP* **03** (2015) 043 [arXiv:1409.1571] [INSPIRE].

[105] I. Asiáin, D. Espriu and F. Mescia, *Introducing tools to test Higgs boson interactions via WW scattering: One-loop calculations and renormalization in the Higgs effective field theory*, *Phys. Rev. D* **105** (2022) 015009 [arXiv:2109.02673] [INSPIRE].

[106] R. Gómez-Ambrosio, F.J. Llanes-Estrada, A. Salas-Bernárdez and J.J. Sanz-Cillero, *SMEFT is falsifiable through multi-Higgs measurements (even in the absence of new light particles)*, *Commun. Theor. Phys.* **75** (2023) 095202 [arXiv:2207.09848] [INSPIRE].

[107] R. Gómez-Ambrosio, F.J. Llanes-Estrada, A. Salas-Bernárdez and J.J. Sanz-Cillero, *Distinguishing electroweak EFTs with $WLWL \to n \times h$*, *Phys. Rev. D* **106** (2022) 053004 [arXiv:2204.01763] [INSPIRE].

[108] A. Dedes et al., *Feynman rules for the Standard Model Effective Field Theory in R_ξ-gauges*, *JHEP* **06** (2017) 143 [arXiv:1704.03888] [INSPIRE].

JHEP11(2023)158

[109] ATLAS collaboration, *Measurement and interpretation of same-sign W boson pair production in association with two jets in pp collisions at $\sqrt{s} = 13$ TeV with the ATLAS detector*, ATLAS-CONF-2023-023, CERN, Geneva (2023).

[110] ATLAS collaboration, *Search for pair-production of vector-like quarks in pp collision events at $\sqrt{s} = 13$ TeV with at least one leptonically decaying Z boson and a third-generation quark with the ATLAS detector*, *Phys. Lett. B* **843** (2023) 138019 [arXiv:2210.15413] [INSPIRE].

[111] ATLAS collaboration, *Search for heavy diboson resonances in semileptonic final states in pp collisions at $\sqrt{s} = 13$ TeV with the ATLAS detector*, *Eur. Phys. J. C* **80** (2020) 1165 [arXiv:2004.14636] [INSPIRE].

[112] F. Arco, D. Domenech, M.J. Herrero and R.A. Morales, *Nondecoupling effects from heavy Higgs bosons by matching 2HDM to HEFT amplitudes*, *Phys. Rev. D* **108** (2023) 095013 [arXiv:2307.15693] [INSPIRE].

[113] K. Hartling, K. Kumar and H.E. Logan, *The decoupling limit in the Georgi-Machacek model*, *Phys. Rev. D* **90** (2014) 015007 [arXiv:1404.2640] [INSPIRE].

JHEP11(2023)158